PHILOSOPHICAL TRANSACTIONS OF THE ROYAL SOCIETY A
MATHEMATICAL, PHYSICAL & ENGINEERING SCIENCES

Turbulence modelling for separated flows with anisotropy-resolving closures

Michael A. Leschziner

Phil. Trans. R. Soc. Lond. A 2000 **358**, 3247-3277
doi: 10.1098/rsta.2000.0707

10.1098/rsta.2000.0707

THE ROYAL SOCIETY

Turbulence modelling for separated flows with anisotropy-resolving closures

By Michael A. Leschziner

Department of Engineering, Queen Mary, University of London, London E1 4NS, UK

This paper discusses aspects of modelling turbulent flows, featuring curvature, impingement and separation, with statistical second-moment closure and nonlinear eddy-viscosity models. Both modelling approaches are first reviewed, with particular emphasis placed on the illumination of some of the mechanisms by which the alternative model forms capture the interactions between particular types of strain and the turbulence field. As part of the review, recent modelling developments, directed especially towards the prediction of physically complex flows, are presented and discussed. Finally, the predictive performance of selected models is illustrated by way of computational solutions and related comparisons with experimental data for five flows, three two dimensional and two three dimensional, all involving separation from continuous surfaces.

Keywords: turbulent separated flow; turbulence modelling; turbulence anisotropy; Reynolds-stress models; nonlinear eddy-viscosity models

1. Introduction

Recent advances in grid generation now allow the flow domain around a complete aircraft to be covered with an unstructured mesh in a matter of one CPU hour on a medium-power workstation. Corresponding progress in numerical approximation schemes, implicit solvers, multi-grid/multi-level acceleration, grid-to-flow adaptation and parallel computing also permits highly accurate numerical solutions to be obtained economically for some restricted groups of flows in which the accuracy of the solution does not rely on closure models that approximate turbulence and associated transport phenomena. Some high-speed, nearly inviscid aeronautical flows, and a smaller number of turbomachine-blade flows in 'design' (low-load) conditions, tend to fall into the above category. At the other extreme is the group of fundamentally important turbulent or transitional flows at relatively low Reynolds numbers, especially those near walls, which can now be fully resolved by *direct numerical simulation* (DNS). While DNS is far too costly for practical flows,† it allows insight to be gained into the detailed physics of turbulence. It also provides accurate and highly resolved statistical data, which have been extensively exploited in recent years for turbulence-model construction, calibration and even validation.

† 'A rough estimate, based on current algorithms and software, indicates that even with a supercomputer capable of performing 10^{12} Flops, it would take several thousand years [and 10^{16} grid points] to compute the flow [around an aircraft] for one second of flight time' (Moin & Kim 1997).

The large majority of flows encountered in fluids-engineering practice are, at least in terms of flow physics, much more challenging than those mentioned above. The key point of difference is the combination of high Reynolds numbers, complex strain and the large contribution of turbulence transport to the balance of processes dictating the behaviour of the flow and hence the operational characteristics of the associated engineering device. Turbulence is known to react sensitively, in terms of both its intensity and structure, to a whole range of geometric and flow features, including the proximity and orientation of walls, curvature, swirl, rotation, density gradients, acceleration, separation and impingement. The level of difficulty rises dramatically with the inclusion of heat and mass transfer, chemical reaction and multi-phase interaction. Here, too, it is turbulence that poses the main challenges, for the transport of heat, species and phases is largely governed by turbulent mixing.

Practical flows are almost invariably computed by solving Reynolds-averaged† versions of the equations of motion and transport in conjunction with turbulence models. The latter feed into the former information on the magnitude of the turbulent stresses, $\rho\overline{u_i u_j}$, and fluxes, $\rho\overline{u_k \phi}$, that arise from the time-/ensemble-averaging process. Any model, however complex, combines rational concepts with healthy measures of intuition and empiricism, the last derived from a calibration of the model against experimental and/or DNS data for a small number of simple key flows. *Large eddy simulation* (LES) is an evolving alternative, but is an expensive approach and is faced with a number of problems associated with spatial filtering, sub-grid-scale modelling, near-wall resolution (especially in the semi-viscous sublayer), and high sensitivity to grid quality (aspect ratio, skewness and spatial rate of expansion).

There are literally dozens of turbulence models, and these differ greatly in terms of their origin, the underlying concepts and the route to their derivation and calibration, their mathematical complexity, their intended range of applicability and their sensitivity to different flow features. To some extent, this proliferation reflects the omission of important generic mechanisms from the turbulence-model equations prior to their closure: in general, the simpler a model is, the more of the fundamental physics is excluded and the greater its reliance is on calibration, which inevitably constrains the model's generality. The application of such simple models to a broad range of flows brings to light, as anticipated, weaknesses and defects (real as well as false) that tend to be addressed by the addition of correction terms and functions and the adjustment of numerical constants. This then gives rise to whole families of models which are, in effect, variants of related parent or 'standard' models. 'Simple' models are taken here to be those based on the linear stress–strain or Boussinesq relationships. More complex and potentially general modelling approaches are based on second-moment closure and nonlinear eddy-viscosity formulations, and these are the ones on which the present paper focuses in an effort to indicate recent developments.

Numerous validation studies provide sufficient evidence to support the conclusion that no single model, however complex and 'general', is able to return a wholly satisfactory behaviour across even a major range of flow conditions. The key objective of any turbulence-modelling effort directed towards general flows is, however, to achieve maximum applicability by minimizing the impact of closure approximations and by retaining as many as possible of the rational and exact elements underpinning the model. On the other hand, the more complex a model is, the more computationally

† Taken here to include time, ensemble and mass averaging.

demanding it tends to be, due to a combination of increased mathematical complexity and disadvantageous numerical properties arising from nonlinearity and inter-equation coupling. Hence, turbulence modelling is often an exercise of compromise.

Assessing the validity of turbulence models by reference to experiments outside the range of those used for model calibration is a crucial part of the modelling process as a whole. This can be a difficult exercise often fraught with uncertainties, even if conducted within extensive and closely controlled collaborative efforts, which are common in Europe (see, for example, Haase *et al*. 1993, 1996). Principal issues affecting validation are numerical accuracy, grid density and disposition, accuracy and completeness of boundary conditions, accuracy of the experimental data, consistency of the dimensionality of the computation with that of the experiment, wind-tunnel-blockage effects, choice of flow properties used for validation (e.g. global as opposed to local) and, not to be ignored, blunders and coding errors. Boundary conditions present particular problems, for they can rarely be extracted for all transported quantities from the experimental data. Indeed, there are many instances in which a major proportion of the boundary conditions needs to be estimated (almost guessed) on the basis of reasonable physical considerations. Examples are the absence of flow inlet conditions for turbulent correlations governed by transport equations, especially in the context of second-moment closure, entrainment conditions along artificial boundaries placed within the flow and far-field boundaries surrounding aerofoils and wings. In such cases, it is essential to place the computational boundaries at positions sufficiently far from the 'active' flow region of primary interest so as to minimize the sensitivity of the flow in this region to changes in the boundary conditions. The treatment of wall conditions is often a serious source of uncertainties, although these do not strictly arise from the boundary conditions (zero slip and impermeability), but rather from the manner in which the turbulence model accounts for the influence of viscosity in the semi-viscous near-wall region.

Validating advanced, anisotropy-resolving models of the type reviewed herein poses particular problems. Not only are these closures especially complex, in terms of their mathematical structure, and numerically difficult to implement, they also require finer grids than those for simpler models, considerably greater CPU resources and more extensive and better resolved experimental data and boundary conditions. A further difficulty arises from the unavoidable lack of experience with any one of these models due to the small number of groups involved in constructing and testing such models. Experience shows that even large-scale collaborative studies tend to offer only few opportunities to reliably cross-check the validity of the implementation of any one particular model, especially if it is of a more complex type, by reference to identical test-case specifications.

In what follows, this paper reviews some recent developments in the area of second-moment and nonlinear eddy-viscosity modelling, and presents selected solutions for some challenging separated flows, which illustrate model performance and the problems encountered in efforts to derive definitive conclusions.

2. Second-moment equations and implied stress–strain linkage

The large majority of models used in practical computational schemes for engineering flows are based on the linear 'Boussinesq' stress–strain relationships,

$$-\overline{u_i u_j} = \nu_t \left(\frac{\partial U_i}{\partial x_j} + \frac{\partial U_j}{\partial x_i} \right) - \tfrac{1}{3}\overline{u_k u_k}\delta_{ij}, \tag{2.1}$$

PHILOSOPHICAL TRANSACTIONS OF THE ROYAL SOCIETY A MATHEMATICAL, PHYSICAL & ENGINEERING SCIENCES

in conjunction with the isotropic eddy viscosity, ν_t, which is typically evaluated from the turbulence energy k and its rate of dissipation ε through $c_\mu k^2/\varepsilon$. These perform well in thin shear flows in which the shear stress is the only dynamically important component of the stress tensor, but often perform poorly in high curvature, separation, recirculation, impingement and swirl. Predictive defects repeatedly observed in computations of complex flows include excessive shear stress, particularly in curved shear layers and in the presence of adverse pressure gradient; suppression of separation along curved walls; grossly excessive levels of turbulence in regions of stagnation and impingement; wrong response to swirl; insensitivity of turbulence transport to density stratification; grossly excessive heat transfer in reattachment regions; and suppression of periodic motions induced by intrinsic instabilities (e.g. shedding from bluff bodies). The cause of many (but not all) problems is that equation (2.1) gives a seriously erroneous linkage between the stresses and strain components and fails to represent the substantial difference in directional alignment between the principal stresses and strains.

The physically correct linkage between stresses and strains is implicit in the equations governing the evolution of the Reynolds stresses, which may be derived exactly from the Navier–Stokes equations and their Reynolds-averaged form. Written symbolically, the Reynolds-stress equations for incompressible flow are:

$$\frac{\mathrm{D}\,\overline{u_i u_j}}{\mathrm{D}\,t} = P_{ij} + d_{ij} + \Phi_{ij} - \varepsilon_{ij}, \tag{2.2}$$

where the left-hand side represents convection, and the four terms on the right-hand side represent production, diffusion, redistribution and dissipation, respectively. Equation (2.2), when written in its full form, reveals the intricate interaction between the stresses and the processes sustaining turbulence. It also provides a partial answer to the question of why eddy-viscosity models (EVMs) are observed to return a credible representation of the mean flow in a fair number of flows, especially those which fall into the category of thin shear flows. Thus, in the case of simple, two-dimensional shear, the exact equation governing the shear stress is

$$\frac{\mathrm{D}\,\overline{uv}}{\mathrm{D}\,t} = -\overline{v^2}\frac{\partial U}{\partial y} + \overline{\frac{p}{\rho}\left(\frac{\partial u}{\partial y} + \frac{\partial v}{\partial x}\right)} - \frac{\partial}{\partial y}\left(\overline{uv^2} + \frac{\overline{pu}}{\rho}\right) - \varepsilon_{12}. \tag{2.3}$$

This stress is the only one which has any relevance to the behaviour of the mean flow. To a first approximation, it may be supposed that the shear stress is proportional to its rate of generation multiplied by a turbulent time-scale:

$$-\overline{uv} \propto \overline{v^2}\frac{\partial U}{\partial y}\frac{k}{\varepsilon}, \tag{2.4}$$

which is consistent with the eddy-viscosity relation (2.1), the eddy-viscosity being a constant times $\overline{v^2}k/\varepsilon$. However, this simple stress–strain linkage does not extend to complex strain fields and cannot be generalized in the form of (2.1) without serious conflict with reality. In particular, equation (2.1) implies that the eigenvectors of the anisotropy tensor $(\overline{u_i u_j}/k - \frac{2}{3}\delta_{ij})$ and the strain tensors are directionally aligned, which is far from true in complex strain.

A key to understanding the relationship between stresses and strains and to identifying the origin of several phenomena that the eddy-viscosity concept is unable to represent is the exact stress-production terms arising in the stress-transport equations (2.2). In terms of Cartesian tensor notation, the stresses $\overline{u_i u_j}$ are produced at a rate:

$$P_{ij} = -\overline{u_i u_k}\frac{\partial U_j}{\partial x_k} - \overline{u_j u_k}\frac{\partial U_i}{\partial x_k}. \tag{2.5}$$

Since the level of generation has, as one would expect, a dominant influence on the associated stresses, it follows that P_{ij} is crucial to the resolution of *stress anisotropy*. The importance of stress anisotropy to mean-field characteristics emerges from considering the response of generation to particular strain or body-force types, each viewed in isolation. This is done below for the examples of flow curvature, system rotation and normal straining. Analogous arguments may be applied to swirl, heat transfer and buoyancy, among others.

In two-dimensional flow, described either within a Cartesian framework or in terms of streamline-oriented coordinates with radius of curvature R, the exact production of the shear stress is given by

$$\left.\begin{aligned} P_{12} &= -\overline{u_2^2}\frac{\partial U_1}{\partial x_2} - \overline{u_1^2}\frac{\partial U_2}{\partial x_1}, \\ \text{or}\quad P_{12} &= -\overline{v_r^2}\frac{\partial U_\theta}{\partial R} + (2\overline{u_\theta^2} - \overline{u_r^2})\frac{U_\theta}{R}. \end{aligned}\right\} \tag{2.6}$$

Streamwise curvature is essentially expressed by the secondary strain $\partial U_2/\partial x_1$ or U_θ/R. In any shear layer, normal-stress anisotropy is high, since the only normal stress generated by shear is that aligned with the streamwise direction. In a wall-bounded shear layer, the wall-normal stress is only a small fraction (typically 25%) of the one in the streamwise direction. It is thus evident that curvature strain in a boundary layer has a disproportionately large influence on the level of shear-stress production and, hence, on the shear stress itself. In the case of a boundary layer on a convex wall, $\partial U_2/\partial x_1$ is negative, and the overall result is a considerable attenuation in the shear stress. This attenuation is further accentuated by the fact that convex curvature tends to reduce $\overline{u_2^2}$ relative to $\overline{u_1^2}$, because

$$P_{22} = -2\overline{u_1 u_2}\frac{\partial U_2}{\partial x_1} \tag{2.7}$$

is negative. An eddy-viscosity model is clearly unable to capture the above interaction, unless sensitized to curvature in an ad hoc manner by some form of a Richardson number that involves the ratio $(U_\theta/R)/(\partial U_\theta/\partial r)$ or a variation thereof.

System rotation gives rise to a body force which interacts with turbulence so as to damp it in some parts of the flow and to amplify it in others, depending upon the orientation (sign) of the strain relative to the rotation vector. This interaction is particularly relevant to turbomachine aerodynamics. It may be shown that rotation introduces into the Reynolds-stress-transport equations the additional exact body-form term:

$$F_{ij} = -2\Omega_p(\varepsilon_{ipq}\overline{u_q u_j} + \varepsilon_{jpq}\overline{u_p u_i}), \tag{2.8}$$

where ε_{ipq} is the alternating third-rank unit tensor. In the simple case of a fully developed flow in a channel rotating anticlockwise in orthogonal mode $\Omega_p = \Omega_3 = \Omega$, relations (2.5) and (2.8) simplify to:

$$\left.\begin{aligned} F_{22}+P_{22} &= -4\Omega\overline{uv}, \\ F_{11}+P_{11} &= -2\overline{uv}\frac{\partial U}{\partial y}+4\Omega\overline{uv}, \\ F_{12}+P_{12} &= -\overline{v^2}\frac{\partial U}{\partial y}-2\Omega(\overline{u^2}-\overline{v^2}). \end{aligned}\right\} \tag{2.9}$$

As the shear stress is negative on the pressure side (the shear strain being positive) and positive on the suction side, (2.9) implies that rotation amplifies (destabilizes) turbulence on the pressure side and damps it on the suction side, leading to an asymmetric velocity profile and higher level of skin friction on the former relative to the latter. This is precisely in accord with experimental observation and DNS data, and is a feature which no linear eddy-viscosity model is able to reproduce, unless sensitized to rotation in an ad hoc fashion through, say, the Rossby number $\Omega/(\partial U/\partial y)$.

Eddy-viscosity models (EVMs) have arisen from and have been calibrated by reference to flows which are strongly sheared. Applying these models to flows in which compressive or extensive straining dominates tends to result in physically unrealistic behaviour. To illustrate this fact, attention is directed towards the production of turbulence energy $P_k = 0.5(P_{11}+P_{22}+P_{33})$:

$$P_k = -\overline{u_1^2}\frac{\partial U_1}{\partial x_1}-\overline{u_2^2}\frac{\partial U_2}{\partial x_2}-\overline{u_1u_2}\left(\frac{\partial U_1}{\partial x_2}+\frac{\partial U_2}{\partial x_1}\right). \tag{2.10}$$

Substitution of equation (2.1) into equation (2.10) gives

$$P_k = \nu_t S^2, \tag{2.11}$$

where $S^2 = S_{ij}S_{ij}$: the autoproduct of the strain tensor. Because of the mass-continuity constraint (in incompressible flow), the first two terms in equation (2.10), involving the normal stresses as multipliers, counteract each other. In fact, the production can easily become *negative* if the negative normal strain is multiplied by the higher of the two normal stresses, with anisotropy being large. When the Boussinesq stress–strain relations are used, however, as is done in (2.10), the production rate becomes quadratic in the strain, and the correct linkage to the normal stresses and strains is lost. Hence, eddy-viscosity models, which feature the turbulence-energy-transport equation, tend to return excessive levels of energy and thus turbulence diffusion in the presence of strong compressive strains. A different perspective of the same defect is offered upon introducing a turbulence time-scale t_0 and velocity scale u_0 and noting (say, from equation (2.5)) that the turbulence production is of the order

$$P_k = O(u_0^2 S t_0), \tag{2.12}$$

while, on dimensional grounds,

$$\nu_t = O(u_0^2 t_0). \tag{2.13}$$

Thus, a combination of equations (2.13) and (2.11) and a comparison of the result with equation (2.12) shows that the eddy-viscosity form (2.11) has the wrong (i.e.

quadratic rather than linear) dependence on S. This has motivated several non-standard eddy-viscosity proposals in which ν_t is made to depend on S as $1/S$, via the coefficient c_μ, a topic which will be considered in greater detail later.

There are many manifestations of the defect rooted in equation (2.11), among them the suppression of separation from the leading edge of aerofoils and turbomachine blades, the underestimation of separation from sharp corners or edges of obstacles on which the flow impinges, and the prediction of seriously excessive wall heat transfer at impingement points. Hence, the ability of a model to distinguish between the effects of shear and irrotational strain may be of crucial importance to the primary operational characteristics of fluid-flow equipment.

3. Second-moment closure

The considerations in the previous section justify the claim that the most rational approach to constructing a turbulence model intended to possess wide-ranging applicability should proceed via the exact set (2.2), which is the basis of *second-moment closure*. The term *closure* gives expression to the fact that diffusion, redistribution and dissipation need to be approximated, a process substantially aided in recent years by a growing body of accurate and detailed DNS data (Spalart 1988; Spalart & Baldwin 1989; Kim *et al*. 1987; Eggels *et al*. 1994; Le & Moin 1994).

With attention initially restricted to high-*Re* flow regions, applicable when the turbulent Reynolds number exceeds $O(100)$, stress diffusion (which is rarely a dominant process) is usually approximated by the *generalized gradient diffusion hypothesis* (GGDH) of Daly & Harlow (1970):

$$d_{ij} = \frac{\partial}{\partial x_k}\left(c_s \overline{u_k u_\ell}\frac{k}{\varepsilon}\frac{\partial \overline{u_i u_j}}{\partial x_\ell}\right). \tag{3.1}$$

More complex forms of (3.1) exist, but are not demonstrably superior (see, for example, Demuren & Sarkar 1993) and have rarely been used. In the exact equations (2.2), the dominant fragment is $\partial(\overline{u_i u_j u_k})/\partial x_k$, with pressure diffusion being sub-ordinate (estimated by Lumley (1978) to be *ca.* 20%). Some attempts have thus been made to determine the triple correlations from third-moment closure, but this has not generally been found to be a profitable route. One notable exception arises in highly stratified shear flows in which the diffusion of stresses and fluxes is extremely important (see Craft *et al*. 1997*a*).

At high Reynolds numbers, dissipation is usually assumed to be isotropic, because it occurs at eddy length-scales which tend to be very much smaller than the scales of the large energetic eddies, which are sensitive to the mean strain (and hence to its orientation), the ratio of the scales being of the order of $Re^{3/4}$. Isotropy in the dissipative scales implies:

$$\varepsilon_{ij} = \tfrac{1}{3}\varepsilon\delta_{ij}, \tag{3.2}$$

in which ε is the dissipation rate of turbulence energy. This approximation is inadequate close to the wall, where length-scales are generally small and anisotropy is large. Proposals have thus been made (in Launder & Tselepidakis (1993) and Hanjalić & Jakirlić (1993), for example) to sensitize ε_{ij}, in an algebraic fashion, to invariants of the stress anisotropy $a_{ij} = (\overline{u_i u_j}/k - \tfrac{2}{3}\delta_{ij})$,

$$A_2 = a_{ij}a_{ij}, \qquad A_3 = a_{ij}a_{jk}a_{ki}, \qquad A = 1 - \tfrac{9}{8}(A_2 - A_3), \tag{3.3}$$

or the dissipation anisotropy $e_{ij} = (\varepsilon_{ij}/\varepsilon - \frac{2}{3}\delta_{ij})$,

$$E_2 = e_{ij}e_{ij}, \qquad E_3 = e_{ij}e_{jk}e_{ki}, \qquad E = 1 - \tfrac{9}{8}(E_2 - E_3). \tag{3.4}$$

From a physical point of view, A_2, A_3 and A may be related to structural features of turbulence, especially its componentality. Thus, $A = 1$ identifies isotropic turbulence ('spherical' eddies), while $A = 0$ characterizes two-component turbulence ('flat' eddies, say, near a wall or a sharp fluid–fluid interface). Moreover, negative values for A_3 characterize 'saucer'-shaped eddies, while positive values indicate 'sausage'-shaped structures. A model widely used to represents the anisotropic dissipation is

$$\varepsilon_{ij} = \tfrac{2}{3} f_\varepsilon \delta_{ij}\varepsilon + (1 - f_\varepsilon)\varepsilon^*_{ij}, \tag{3.5}$$

where ε^*_{ij} are the wall-limiting values of ε_{ij}, which can be obtained readily by kinematic arguments (Launder & Reynolds 1983). The 'blending' function f_ε varies from model to model—there are at least five forms (see Hanjalić 1994)—and its subjects are A and/or E and/or Re_{t}. Apart from securing the correct wall-limiting behaviour of ε_{ij} and introducing shear-stress dissipation, equation (3.5) also ensures that dissipation of the wall-normal intensity is 'shut off' as turbulence approaches the two-component near-wall limit. This is an important element of any model designed to satisfy *realizability*, a property which includes the unconditional satisfaction of $\overline{u^2_\alpha} \geqslant 0$ (with α denoting the principal directions).

Alongside dissipation, the redistribution or 'pressure–strain' term Φ_{ij} presents the modeller with the biggest challenge in the context of second-moment closure. This term vanishes upon the contraction $k = \frac{1}{2}\overline{u_i u_j}\delta_{ij}$ (strictly, in incompressible flow only) and thus becomes irrelevant in closures based on the turbulence energy or a surrogate scalar. In second-moment closure, however, this term controls the redistribution of turbulence energy among the normal stresses—a process driving turbulence towards a state of isotropy—as well as the reduction in the shear stresses in harmony with the isotropization process. It only requires reference to equation (2.4) to appreciate that the correct resolution of the individual normal stresses is of crucial importance in the context of second-moment closure. In simple shear flow, to which equation (2.4) pertains, the shear stress is clearly directly proportional to the transverse normal stress $\overline{v^2}$, a stress which is not generated in simple shear, but is only finite because of the redistribution process effected by Φ_{ij}.

It can be shown analytically that the redistribution process consists of two major constituents, one involving an interaction between turbulent quantities only ($\Phi_{ij,1}$ and termed *slow*) and the other involving an interaction between mean strain and turbulence fluctuations ($\Phi_{ij,2}$ and termed *rapid*). This fact has led most modellers to make separate proposals for these two fragments. The simplest proposal forms, used for most complex-flow computations, are the linear relations by Rotta (1951) and Gibson & Launder (1978), respectively:

$$\left.\begin{aligned} \Phi_{ij,1} &= \frac{-c_1\varepsilon}{k}(\overline{u_i u_j} - \tfrac{1}{3}\delta_{ij}\overline{u_k u_k}), \\ \Phi_{ij,2} &= -c_2(P_{ij} - \tfrac{1}{3}\delta_{ij}P_{kk}). \end{aligned}\right\} \tag{3.6}$$

Fu *et al.* (1987*b*) have shown, by reference to swirling flow, that the above form of $\Phi_{ij,2}$ is not frame invariant, but that invariance is assured if the body-force-related production terms F_{ij} and the convection tensor are included to give the form:

$$\Phi_{ij,2} = -c_2([P_{ij} + F_{ij} - \tfrac{1}{3}\delta_{ij}(P_{kk} + F_{kk})] - (C_{ij} - \tfrac{1}{3}\delta_{ij}C_{kk})). \tag{3.7}$$

Although this combined 'linear' model satisfies the basic requirement of steering turbulence towards isotropy, the isotropization process is far too intense at the high levels of anisotropy prevailing near the wall or free liquid surface. As the wall is approached, turbulence tends towards a two-dimensional state ($A = 0$), and redistribution must vanish to allow this state to be achieved. By intensifying the isotropization process as the wall is approached, the linear model does not merely fail to represent the physical process correctly, but can lead to one of the principal normal stresses becoming negative, a condition violating *realizability*.

Correcting the above weakness, within the linear framework, relies on the introduction of elaborate and influential ad hoc terms (Shir 1973; Gibson & Launder 1978; Craft & Launder 1992), which counteract the isotropization process in proportion to the distance from the wall, normalized by the turbulent length-scale $k^{3/2}/\varepsilon$. For example, for a shear layer along a single horizontal wall, the correction terms damping the linear isotropization of the wall-normal stress $\overline{v^2}$ are:

$$\left.\begin{aligned} \Phi^{\mathrm{w}}_{22,1} &= -c^{\mathrm{w}}_1 \frac{4}{3}\frac{\varepsilon}{k}\overline{v_2}\frac{k^{1.5}/\varepsilon}{c_\mu^{-3/4}\kappa y}, \\ \Phi^{\mathrm{w}}_{22,2} &= 2c^{\mathrm{w}}_2(P_{22} - \tfrac{2}{3}P_k)\frac{k^{1.5}/\varepsilon}{C_\mu^{-3/4}\kappa y}. \end{aligned}\right\} \tag{3.8}$$

In addition, the redistribution process needs to be sensitized to inhomogeneity, associated with large strain gradients, and to anisotropy invariants, especially in low-*Re* forms which allow the model to be used down to the wall (So *et al*. 1991; Launder & Shima 1989; Ince *et al*. 1994; Jakirlić & Hanjalić 1995; Craft & Launder 1996). An example of the latter practice is that of Jakirlić & Hanjalić (1995) who made extensive use of DNS data to calibrate their linear low-*Re* model and use

$$\left.\begin{aligned} c_1 &= 2.5A[\min(0.6, A_2)]^{1/4}f + \sqrt{A}E^2, \\ c_2 &= 0.8A^{1/2}, \end{aligned}\right\} \tag{3.9}$$

where f is a function of the turbulent Reynolds number Re_{t}. Similarly, c^{w}_1 and c^{w}_2 are sensitized to A, A_2 and Re_{t}.

An alternative, recently proposed by Durbin (1993), introduces an *elliptic relaxation equation* of the form

$$L^2\nabla^2\frac{\phi^{\mathrm{c}}_{ij}}{k} - \frac{\phi^{\mathrm{c}}_{ij}}{k} = \frac{\phi_{ij}}{k}, \tag{3.10}$$

where ϕ^{c}_{ij} is the wall-corrected form of the standard (uncorrected) ϕ_{ij}, L is the turbulence length-scale and ∇^2 is the elliptic operator. Equation (3.10) steers ϕ_{ij} towards the correct wall values, prescribed as boundary conditions for ϕ^{c}_{ij}.

From a fundamental point of view, as well as on practical grounds, the use of wall corrections is unsatisfactory, not only because of their non-general nature, but also because they rely heavily on the wall distance (y in equation (3.8)). The latter is especially disadvantageous in complex geometries, where the influence of more than one wall needs to be taken into account, and when general non-orthogonal

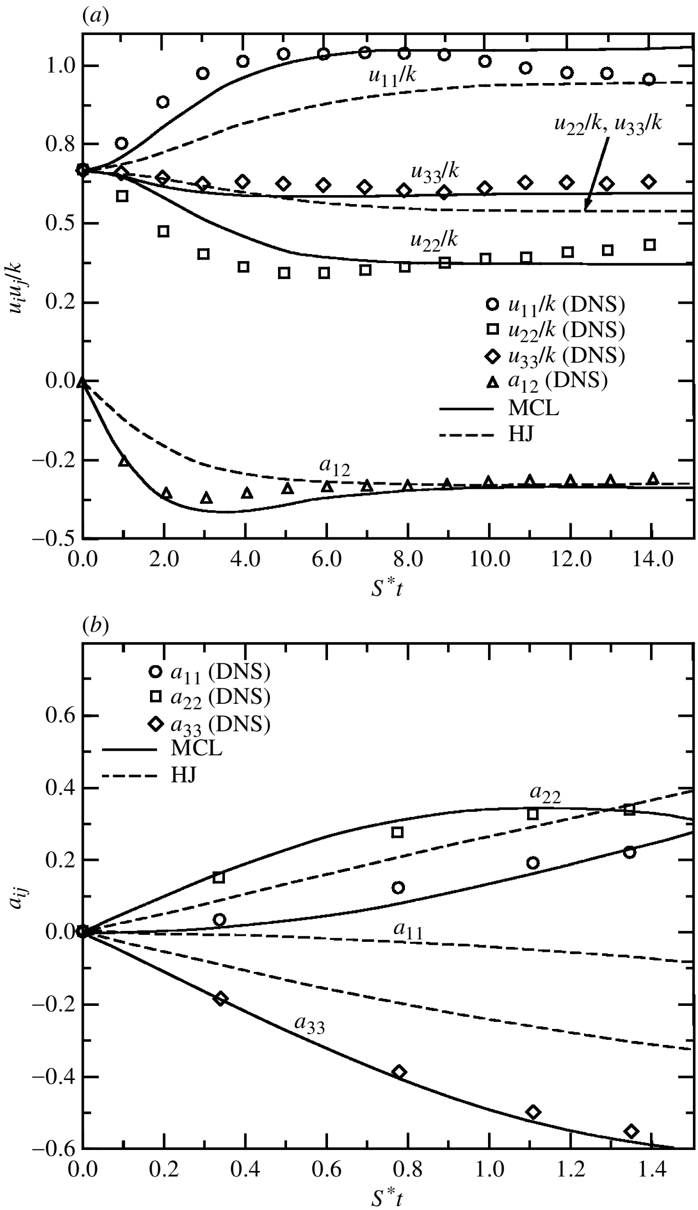

Figure 1. Temporal variations of Reynolds stresses when isotropic turbulence is subjected to homogeneous strain: (*a*) shear and (*b*) plane strain ('HJ' denotes Jakirlić & Hanjalić (1995); 'MCL' denotes (modified) Craft & Launder (1996)).

numerical grids are used. Hence, much of the recent fundamental research in the area of turbulence modelling has been concerned with the construction of *nonlinear* pressure–strain models that satisfy the realizability constraints and do not require wall corrections. Nonlinear models or variants have been proposed by Shih & Lumley (1985), Fu *et al.* (1987*a*) and Speziale *et al.* (1991), Launder & Tselepidakis (1993),

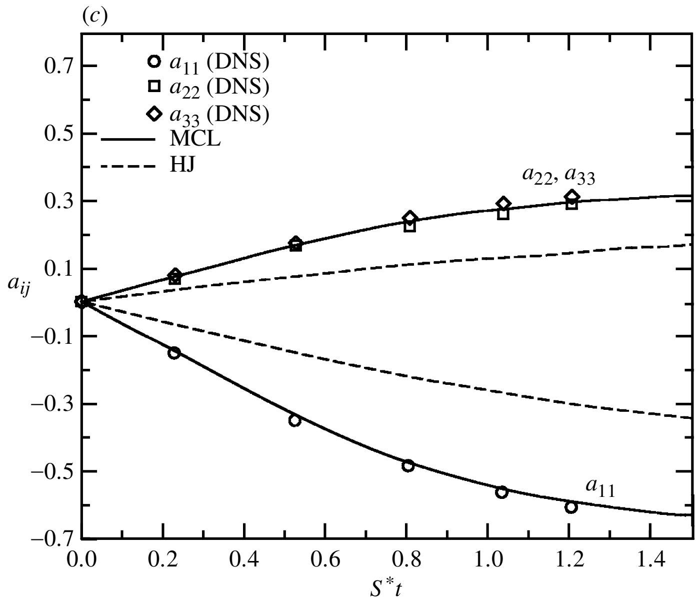

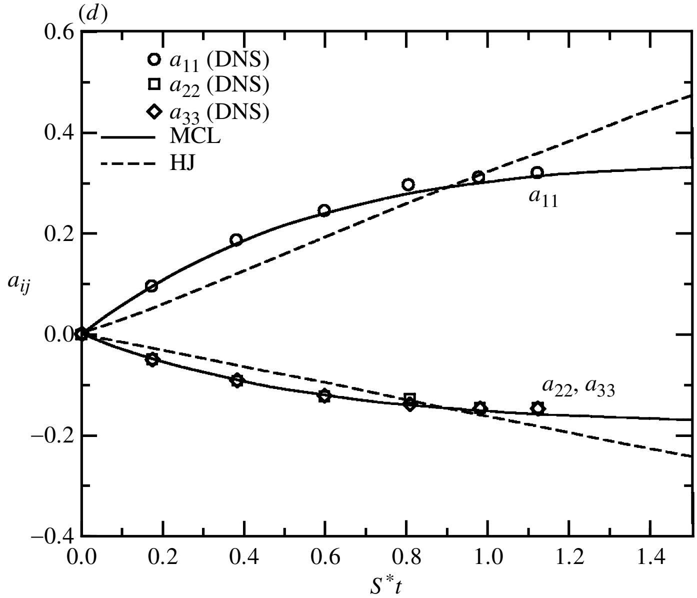

Figure 1. (*Cont.*) (*c*) Axisymmetric contraction and (*d*) axisymmetric expansion.

Craft & Launder (1996), Craft (1998) and Batten *et al.* (1999), the last four being extensions of Fu *et al.*'s model and the very last being a compressibility-generalized variant suitable for shock-affected flows. The models differ in detail and in respect of the order of terms included, but all have arisen from the common approach of proposing nonlinear expansions, in terms of components of the Reynolds-stress tensor $\overline{u_i u_j}$ (or rather the anisotropy tensor, $a_{ij} = (\overline{u_i u_j}/k - \frac{2}{3}\delta_{ij})$) to second- and fourth-rank tensors that arise in the most general *ansatz* for the pressure–strain term prior to its approximation:

$$\Phi_{ij} = \varepsilon A_{ij}(a_{ij}) + k M_{ijk\ell}(a_{ij}) \frac{\partial U_k}{\partial x_\ell}, \tag{3.11}$$

in which the two groups of terms correspond, respectively, to $\Phi_{ij,1}$ and $\Phi_{ij,2}$. The coefficients of the various terms in the expansions for A_{ij} and M_{ijkl} (in terms of a_{ij}) are then determined by imposing necessary kinematic constraints (continuity, symmetry, etc.). Realizability is introduced into some model forms by sensitizing the pressure–strain model to invariants of the stress anisotropy. For example, the model of Speziale *et al.* (1991) involves a quadratic form of $\Phi_{ij,1}$, the linear fragment of which is premultiplied by the coefficient

$$c_1 = 1 + 3.1(A_2 A)^{1/2}. \tag{3.12}$$

The most elaborate model is that of Craft & Launder (1996) and is quadratic in $\Phi_{ij,1}$ and cubic in $\Phi_{ij,2}$, the latter containing six distinct groups of terms and associated coefficients. This model has recently been modified by Batten *et al.* (1999) to apply to shock-affected flows, in view of experience which had revealed that the parent form responds incorrectly to shocks.

The intrinsic predictive quality of the above, most elaborate, framework is reflected by its ability to represent the response of turbulence to different types of strain. This is conveyed by figures 1 and 2, taken from Batten *et al.* (1999). The former gives temporal variations (S^* representing the non-dimensional strain rate) of stresses when isotropic turbulence is subjected to homogeneous shear, plain strain, axisymmetric contraction and axisymmetric expansion. The figure includes two sets of solutions, one obtained with the modified form (Batten *et al.* 1999) of the cubic model of Craft & Launder (1996) and the other with the linear model of Jakirlić & Hanjalić (1995). Predicted variations are compared with DNS data by Matsumoto *et al.* (1991). Figure 2 shows analogous comparisons with DNS data of Lee & Reynolds (1985) for near-wall stress profiles in a channel flow at a Reynolds number, based on friction velocity and channel height, of 180 (the mean Reynolds number being about 5000). Although these strain conditions are far from those encountered in practice, they nevertheless demonstrate the ability of second-moment closure to return key characteristics of strained turbulence, and this is, arguably, a prerequisite for a general applicability of any model across a broad range of strain types.

It must be acknowledged that the above cubic forms continue to rely on wall corrections (or *inhomogeneity* terms), albeit much weaker than those associated with the linear models. To at least avoid reliance on the wall distance, efforts have thus been made to replace the wall-distance parameter in equation (3.8) by local turbulence-structure parameters which indicate the wall proximity by implication. Examples for such parameters are those proposed by Craft & Launder (1996) and Jakirlić (1997),

$$f^{\mathrm{w}} = \frac{1}{c_l} \frac{\partial l}{\partial x_n} \quad \text{or} \quad f^{\mathrm{w}} = \frac{1}{c_l} \frac{\partial A^{1/2} l}{\partial x_n}, \tag{3.13}$$

where $c_l = c_\mu^{-3/4} \kappa$, $l = k^{3/2}/\varepsilon$.

Determining the dissipation rate ε (and, hence, ε_{ij}) is another challenge in the context of second-moment closure. With few exceptions, ε is determined from a single transport equation representing, rather intuitively, a balance between transport,

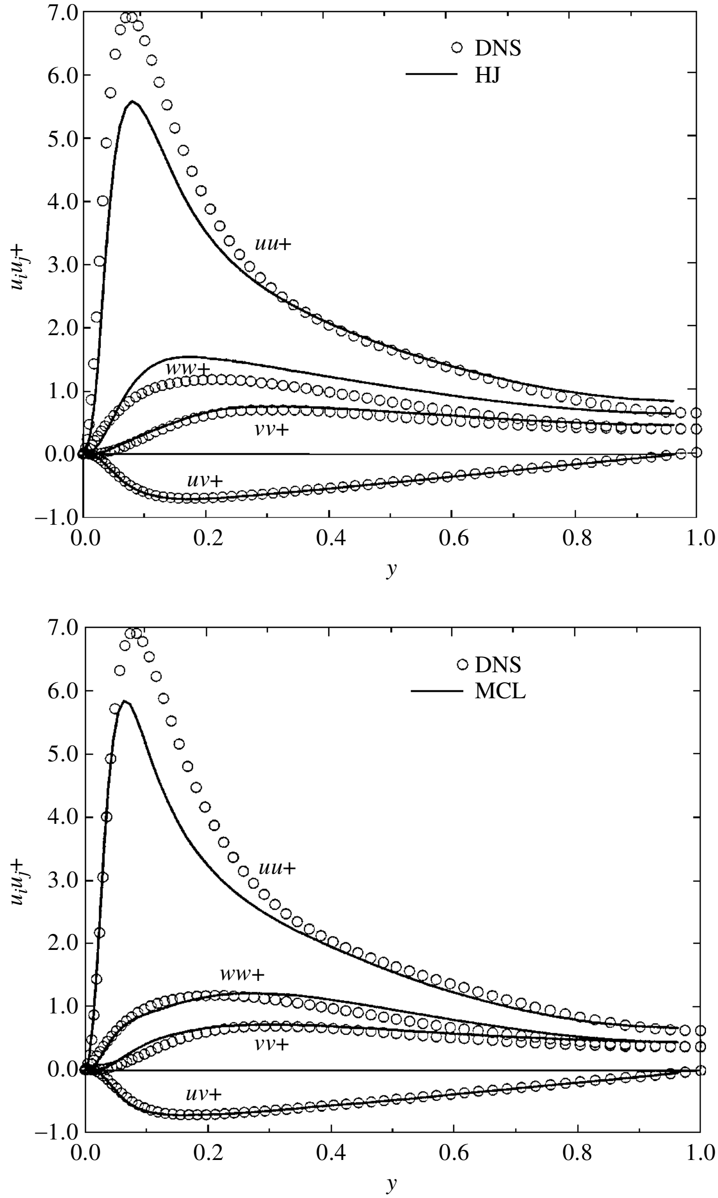

Figure 2. Profiles of Reynolds stresses across half a fully developed channel flow at $Re_\tau = 180$ predicted with second-moment closures (see caption of figure 1 for model designations).

generation and destruction of dissipation:

$$\frac{\partial \rho U_k \varepsilon}{\partial x_k} = \frac{\partial}{\partial x_k}\left(\rho c_t \frac{\overline{u_k u_\ell}}{\varepsilon} k \frac{\partial \varepsilon}{\partial x_\ell}\right) + 0.5\rho\left(\frac{\varepsilon}{k}\right) c_{\varepsilon 1} P_{kk} - \rho c_{\varepsilon 2}\left(\frac{\varepsilon^2}{k}\right) + S_\varepsilon, \tag{3.14}$$

in which S_ε is a model-dependent source-like term containing specific corrections and terms associated with the influence of viscosity on dissipation. Apart from associating the dissipation process with the single macro-length-scale $k^{3/2}/\varepsilon$, the above equation suggests only a very weak sensitivity of dissipation to the structure of turbulence. As turbulence anisotropy increases, especially at walls, the normal components of the dissipation tensor become anisotropic (as expressed by equation (3.5)). A proposal sensitizing the scalar dissipation rate to anisotropy is that of Haroutunian *et al.* (1988), in which $c_{\varepsilon 1} = 1.44$ and $c_{\varepsilon 2} = 1.92$ are replaced by

$$c_{\varepsilon 1} = 1, \qquad c_{\varepsilon 2} = \frac{1.92}{(1 + 0.7AA_2^{1/2})}. \tag{3.15}$$

An apparently intractable defect of the dissipation-rate equation is that it returns excessive levels of turbulent length-scale in boundary layers subjected to adverse pressure gradient. Among other problems, this property results in excessive near-wall shear stress and hence inappropriate suppression of separation from continuous surfaces. This defect is common to both two-equation eddy-viscosity models† and Reynolds-stress models. Within the former framework, Lien & Leschziner (1995) have introduced constraints which, as the wall is approached, drive the length-scale towards the value prescribed algebraically as part of the one-equation model of Norris & Reynolds (1975). However, in most model forms and applications the defect is addressed by introducing, via S_ε in equation (3.14), some variant of the ad hoc correction of Yap (1987), which forces the ε equation to return a length-scale close to the local equilibrium value. An example is the recent variant of Jakirlić & Hanjalić (1995):

$$S_\varepsilon = \max\left(\left[\left(\frac{1}{c_l}\frac{\partial l}{\partial x_n}\right)^2 - 1\right]\left(\frac{1}{c_l}\frac{\partial l}{\partial x_n}\right)^2, 0\right) A\frac{\varepsilon\tilde{\varepsilon}}{k}, \tag{3.16}$$

in which $\tilde{\varepsilon}$ is the homogeneous part of the dissipation ε.

Little has been said so far about accommodating the effects of viscosity in the context of low-*Re* modelling. Most recent models, among them those of Launder & Tselepidakis (1993), So *et al.* (1991), Launder & Shima (1989), Jakirlić & Hanjalić (1995) and Craft & Launder (1996), are low-*Re* variants, allowing an integration through the viscous sublayer. This is an area in which much reliance is placed on recent DNS data for near-wall flows. In essence, different model elements, especially the dissipation equation (via $c_{\varepsilon 1}$, $c_{\varepsilon 2}$ and S_ε), are sensitized to viscosity by way of damping functions with subjects being forms of the turbulent Reynolds number. As the near-wall structure is substantially affected by both inertial and viscous damping, the former provoking strong anisotropy via pressure reflections, low-*Re* extensions involve a functionalization on anisotropy invariants (3.3) as well as viscosity, each expressing a different physical process. The dissipation invariants (3.4) can also be used, as has been done by Jakirlić & Hanjalić (1995). Because the functionalization process is non-rigorous, essentially aiming to make the model return a phenomenological behaviour consistent with experimental or DNS data, there is a considerable amount of ambiguity in extending models to low-*Re* conditions, and thus each model features its own individual sets of functions derived along different routes. Such extensions are not, therefore, considered in detail here.

Although low-*Re* second-moment closure models are beginning to be applied to quite complex two-dimensional and even three-dimensional flows, the desire for rela-

† It can be materially alleviated, however, by a replacement of the ε equation by an analogous equation for the turbulent vorticity ω (see, for example, Wilcox 1994).

tive simplicity and the uncertainties associated with near-wall modelling have encouraged the application of somewhat 'simpler' hybrid models which combine high-*Re* second-moment closure with low-*Re* EVMs, the latter applied to the viscous near-wall layer (Lien & Leschziner 1993, 1995), or even with wall functions (Lien 1992; Leschziner & Ince 1995; Jakirlić 1997). Justification, especially for the former option, is provided by the observation that stress transport is usually uninfluential very close to the wall and that the principal function of the near-wall model is to provide the correct level of the shear stress and wall-normal heat flux.

4. Nonlinear eddy-viscosity models

Second-moment closure has compelling fundamental merits, as well as yielding real predictive benefits in complex two-dimensional and three-dimensional flows. On the other hand, it is mathematically elaborate, numerically challenging and (often) computationally expensive, all regarded as important limitations in the context of industrial CFD. This has thus motivated efforts to construct models which combine the simplicity of the eddy-viscosity formulation with the superior fundamental strength and predictive properties of second-moment closure. These efforts have given rise to the group of *nonlinear* eddy-viscosity models (NLEVMs).

NLEVMs can be traced back to early work by Rivlin (1957), leaning on similarities between the laminar flow of a non-Newtonian fluid and the turbulent flow of a Newtonian fluid, and Pope's (1975) observation that Rodi's (1976) algebraic approximation of the Reynolds-stress-transport model of Launder *et al*. (1975) can be arranged in the explicit form

$$a_{ij} = \sum G^{\lambda} T_{ij}^{\lambda}, \tag{4.1}$$

where T_{ij} is a tensorial power expansion in the strain and vorticity tensors,

$$S_{ij} \equiv \frac{1}{2}\left(\frac{\partial U_i}{\partial x_j} + \frac{\partial U_j}{\partial x_i}\right), \qquad \Omega_{ij} \equiv \frac{1}{2}\left(\frac{\partial U_i}{\partial x_j} - \frac{\partial U_j}{\partial x_i}\right), \tag{4.2}$$

while G^{λ} are coefficients which are functions of vorticity and strain invariants. A first generation of quadratic models emerged through contributions by Saffman (1977), Wilcox & Rubesin (1980) and Speziale (1987). In Speziale's model, for example, the coefficients G^{λ} were simply taken to be powers of the time-scale k/ε so as to achieve dimensional consistency. Since then, a number of models of various complexity and derived along quite different routes have emerged (Yoshizawa 1987; Shih *et al*. 1993; Rubinstein & Barton 1990; Gatski & Speziale 1993; Craft *et al*. 1997*b*; Lien & Durbin 1996; Lien *et al*. 1996; Taulbee *et al*. 1993; Wallin & Johansson 1997; Apsley & Leschziner 1998). Most models are quadratic, while those of Craft *et al*., Lien *et al*. and Apsley & Leschziner are cubic and that of Gatski & Speziale is quartic. These differences in order are of considerable significance. In particular, the cubic fragments play an essential role in capturing the strong effects of curvature on the Reynolds stresses. As regards model origin and derivation, an important distinction arises from the fact that some models (those of Shih *et al*., Lien *et al*. and Craft *et al*., for example) start from a general series-expansion of the Reynolds-stress tensor in terms of strain and vorticity tensors, while others (those of Gatski & Speziale, Apsley & Leschziner, Taulbee *et al*. and Wallin & Johansson) start from an algebraic

Reynolds-stress model. Other routes involve the *direct interaction* approximation adopted by Yoshizawa and the *renormalization group* (RNG) approach taken by Rubinstein & Barton. Most models use constitutive equations which are functions of two turbulence scales (usually k and ε) as well as strain and vorticity invariants. In contrast, one variant of Craft *et al.*'s cubic model makes use of a transport equation for the stress invariant $A_2 = a_{ij}a_{ij}$, while Lien & Durbin's quadratic model depends on the Reynolds stress normal to the streamlines, which is also obtained from a related transport equation.

To a degree, the multiplicity of the NLEVMs published in the literature is indicative of the loss of rigour inherent in moving away from the complete second-moment framework towards a simpler closure level, which necessarily involves more empirical input and greater intuitive content. Clearly, the critical question is whether the simplification is justified in terms of the predictive performance which nonlinear formulations return relative to linear models and second-moment closure. This question cannot be answered categorically, at present, because of insufficient evidence and the diversity of models, each displaying individual predictive characteristics.

Although the rational foundation and derivation of different models can differ greatly, the stress–strain/vorticity constitutive relationship for the quadratic or cubic models to be considered in this paper can be written (for incompressible flow) in the following canonical form:

$$\begin{aligned} a_{ij} = {} & -2c_\mu \frac{k}{\tilde{\varepsilon}} S_{ij} + c_1 \frac{k^2}{\tilde{\varepsilon}^2}(S_{ik}S_{jk} - \tfrac{1}{3}S_{kl}S_{kl}\delta_{ij}) + c_2 \frac{k^2}{\tilde{\varepsilon}^2}(S_{ik}\Omega_{jk} + S_{jk}\Omega_{ik}) \\ & + c_3 \frac{k^2}{\tilde{\varepsilon}^2}(\Omega_{ik}\Omega_{jk} - \tfrac{1}{3}\Omega_{kl}\Omega_{kl}\delta_{ij}) + c_4 \frac{k^3}{\tilde{\varepsilon}^3}(S_{ik}\Omega_{jl} + S_{jk}\Omega_{il})S_{kl} \\ & + c_5 \frac{k^3}{\tilde{\varepsilon}^3}(\Omega_{ik}\Omega_{kl}S_{lj} + \Omega_{jk}\Omega_{kl}S_{li} - \tfrac{2}{3}\Omega_{kl}S_{lm}\Omega_{mk}\delta_{ij}) \\ & + c_6 \frac{k^3}{\tilde{\varepsilon}^3}S_{kl}S_{kl}S_{ij} + c_7 \frac{k^3}{\tilde{\varepsilon}^3}\Omega_{kl}\Omega_{kl}S_{ij}. \end{aligned} \tag{4.3}$$

This expression, which is either the starting point of a nonlinear model or the outcome of certain simplifications introduced into the Reynolds-stress equations, satisfies all requisite symmetry and contraction properties in incompressible flow. It admits models, such as that of Craft *et al.* (1997*b*), where a distinction is made between dissipation rate ε and its homogeneous part $\varepsilon - 2v(\partial k^{1/2}/\partial y)^2$. For most models to be considered here, no such distinction is made.

The mechanism by which NLEVMs represent anisotropy emerges upon considering simple two-dimensional shear in the (x_1, x_2)-plane, in which $\sigma = (k/\varepsilon)(\partial U/\partial y)$ characterizes the strain, for which equation (4.3) yields:

$$\left.\begin{aligned} a_{11} &= \tfrac{1}{12}(c_1 + 6c_2 + c_3)\sigma^2, \\ a_{22} &= \tfrac{1}{12}(c_1 - 6c_2 + c_3)\sigma^2, \\ a_{33} &= -\tfrac{1}{6}(c_1 + c_3)\sigma^2, \\ a_{12} &= -c_\mu\sigma + \tfrac{1}{4}(c_6 + c_7 - c_5)\sigma^3. \end{aligned}\right\} \tag{4.4}$$

This demonstrates that the quadratic terms are responsible for the ability of nonlinear models to capture anisotropy: without these, $\overline{u_\alpha^2} = \tfrac{2}{3}k$, for $\alpha = 1, 2, 3$. Also, by establishing a link between the normal stresses and the shear strain, relations

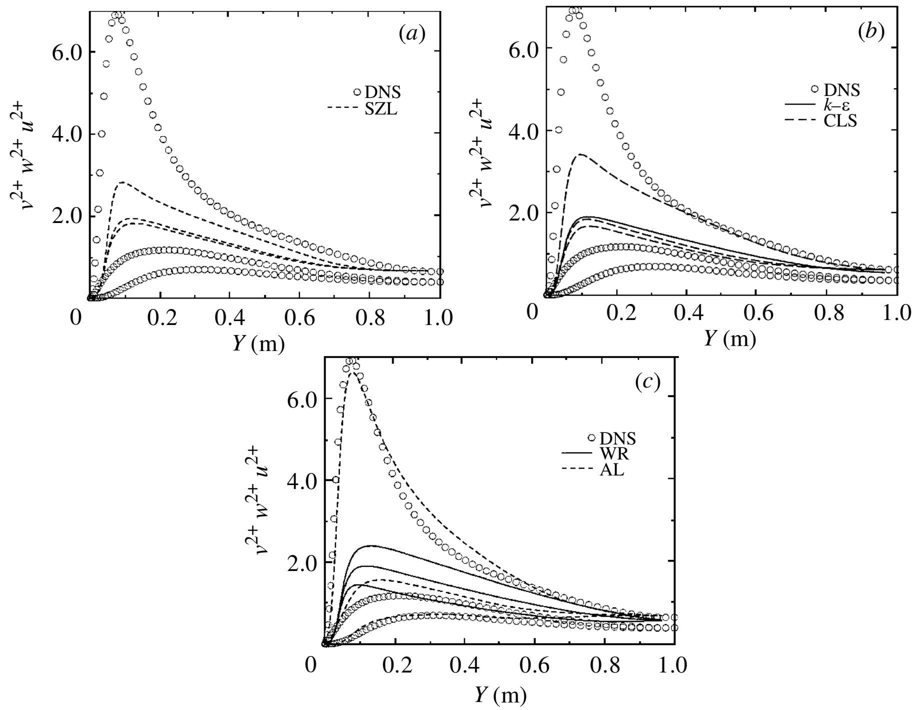

Figure 3. Profiles of Reynolds stresses across half a fully developed channel flow at $Re_\tau = 180$ predicted with nonlinear eddy-viscosity models. WR denotes Wilcox & Rubesin (1980); CLS denotes Craft *et al.* (1997*b*); SZL denotes Shih *et al.* (1993); AL denotes Apsley & Leschziner (1998); k–ϵ denotes the linear EVM.

Table 1. *Equilibrium values of non-dimensional anisotropy and shear stress for homogeneous turbulent shear flow*

	$a_{11,\infty}$	$a_{12,\infty}$	$a_{22,\infty}$	$a_{33,\infty}$	$(Sk/\varepsilon)_\infty$
experiment	0.403	−0.284	−0.295	−0.108	6.08
linear k–ε EVM	0	−0.434	0	0	4.82
WR	0.3	−0.434	−0.3	0	4.82
SZL	0.313	−0.318	−0.19	−0.112	6.56
CLS	0.53	−0.273	−0.307	−0.223	7.66
AL	0.449	−0.276	−0.353	−0.095	6.81

(4.4) are, qualitatively, compatible with statements derived from the Reynolds-stress equations. However, the predictive quality with which any particular nonlinear model resolves anisotropy depends significantly on the calibration of the model's coefficients. This is demonstrated in figure 3, taken from Loyau *et al.* (1998), which compares levels of normal-stress anisotropy predicted by the nonlinear models of Wilcox & Rubesin (1980), Craft *et al.* (1997*b*), Shih *et al.* (1993) and Apsley & Leschziner (1998) with DNS data for channel flow by Kim *et al.* (1987). Table 1, also taken from Loyau *et al.* (1998), shows the equilibrium values of the deviatoric normal stresses and the shear stress when isotropic turbulence is subjected to homogeneous

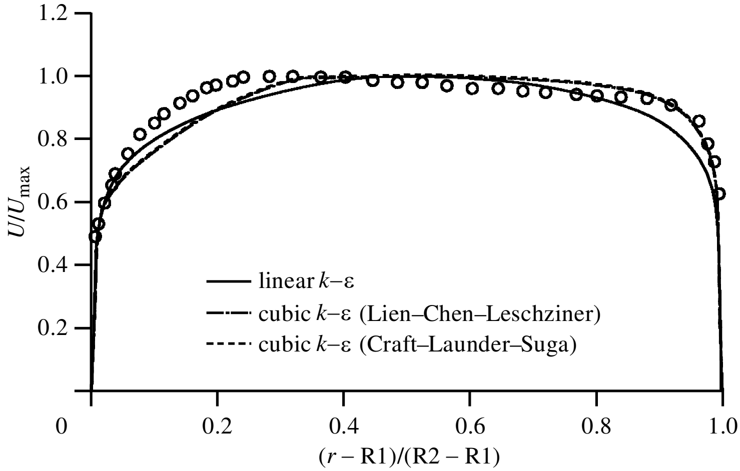

Figure 4. Velocity profiles in fully developed curved channel flow predicted by two cubic eddy-viscosity models in comparison with the linear k–ϵ model.

shear for a long period of time. Predicted values are compared with experimental data by Tavoularis & Corrsin (1981).

The mechanism by which curvature effects are represented transpires from a consideration of the shear stress in two-dimensional shear. Assuming that $c_6+c_7-c_5=0$ (so that the cubic terms play no role in simple shear), relations (4.3) give:

$$a_{12} = -2[c_\mu + \tfrac{1}{4}(c_7 - c_5)(\tilde{S}^2 - \tilde{\Omega}^2)](k/\varepsilon)S_{12}, \tag{4.5}$$

where

$$\tilde{S} = (k/\varepsilon)\sqrt{2S_{ij}S_{ij}}, \qquad \tilde{\Omega} = (k/\varepsilon)\sqrt{2\Omega_{ij}\Omega_{ij}}. \tag{4.6}$$

Result (4.5) highlights the fact that (some of) the cubic fragments can be assimilated into the linear term, and this allows the effects of curvature to be brought out most clearly. Thus, if $c_7 - c_5$ is chosen positive, the shear stress will increase when $\tilde{S}^2 - \tilde{\Omega}^2 > 0$ and will decrease when $\tilde{S}^2 - \tilde{\Omega}^2 < 0$. This effect is illustrated in figure 4, which compares the velocity profiles predicted by the cubic models of Lien *et al.* (1996) and Craft *et al.* (1997*b*) relative to a solution from a linear k–ε model and experimental data of Ellis & Joubert (1974). The effect is qualitatively equivalent to that predicted by the Reynolds-stress transport equations, although, in that case, the sensitivity is brought about by a direct interaction between normal-stress anisotropy and curvature strain, via the stress-generation terms.

There are other consequences that may be derived directly from the canonical form of equation (4.3). Firstly, in two-dimensional flow, the quadratic terms (those multiplied by coefficients c_1, c_2 and c_3) have no *direct* effect on turbulence-energy production. Secondly, again in two-dimensional conditions, the cubic term associated with c_4 vanishes, while the remaining cubic terms are proportional to the mean strain tensor.

Although all cubic models are based on equation (4.3), they differ substantially in detail, especially in respect of the determination of the coefficients c_μ and c_1 to c_7 and the forms of the dissipation equation. Specifically, one of the two models of Craft *et al.* (1997*b*) sensitizes the coefficients to A_2, which is determined from a related

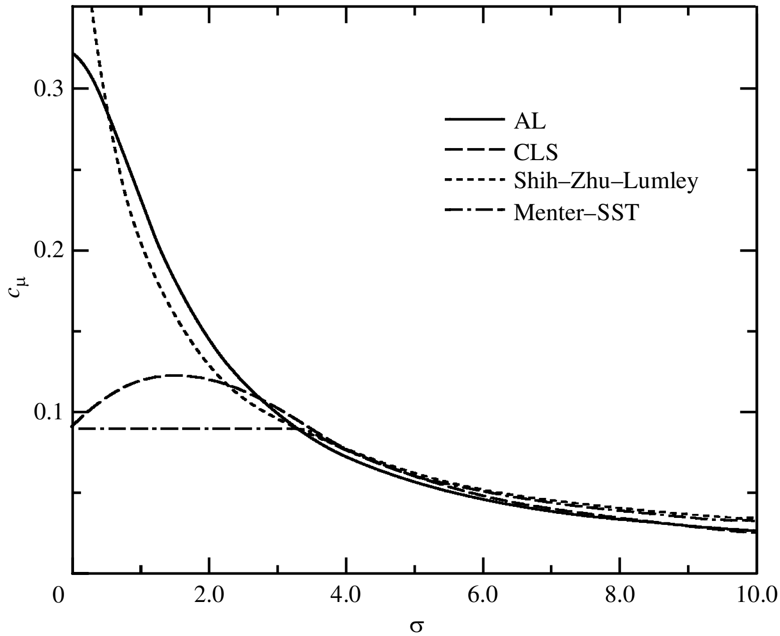

Figure 5. Variation of the eddy-viscosity coefficient c_μ for different nonlinear eddy-viscosity model and Menter's (1994) SST model, as a function of the strain rate $\sigma = k/\epsilon(\partial U/\partial y)$ in homogeneous shear (standard value for linear EVMs is 0.09).

transport equation derived from second-moment closure. Of particular importance is the form of c_μ. In the context of linear two-equation eddy-viscosity models, this coefficient normally takes the value 0.09 (corresponding to $\overline{uv}/k = 0.3$ in equilibrium shear). However, as pointed out earlier in relation to the response of linear eddy-viscosity models to normal straining, by reference to equations (2.11)–(2.13), a constant value of c_μ gives the wrong response to normal straining. Rather, it was argued that c_μ should be proportional to $1/S$. Because the production rate of turbulence energy is not sensitive to the quadratic terms, which allow nonlinear models to represent anisotropy, a similar dependence of c_μ on S is also required in nonlinear models. Figure 5, taken from Loyau *et al*. (1998), shows variations of c_μ with the non-dimensional strain in simple shear, $k/\varepsilon(\partial U/\partial y)$, built into three nonlinear models (AL denotes Apsley & Leschziner (1998) and CLS denotes Craft *et al*. (1997*b*)). As seen, all three models incorporate a similar functional dependence, especially at strain rates exceeding the equilibrium value. In most model variants, c_μ is sensitized to the strain and vorticity invariants, so as to avoid the excessive generation of turbulence energy in stagnation flow. In turbomachine blades, for example, this dependence is crucially important for the prediction of boundary-layer transition, especially on the suction side, following the impingement of the highly turbulent upstream flow on the blade's leading edge.†

† Of course, the manner in which the transition process itself is modelled, especially in off-design conditions in which impingement is often followed by laminar leading-edge separation and turbulent reattachment, is at least of equal importance.

5. Model performance

There must be close to 100 flows which have been subjects of investigations with second-moment and nonlinear eddy-viscosity models, principally in order to evaluate the models' predictive performance characteristics. Most of these flows are (nominally) two-dimensional, some are swirling and many are attached. Arguably, amongst the most challenging flows are those in which separation occurs from a continuous surface. Five such cases are considered here: a two-dimensional flow in an asymmetric plane diffuser (Obi *et al.* 1993), a two-dimensional flow over a compressor-cascade blade (Zierke & Deutsch 1989), a three-dimensional flow around a prolate spheroid (Meier *et al.* 1984), a two-dimensional transonic flow over a circular bump (Bachalo & Johnson 1986), and a three-dimensional transonic flow around a fin–flat-plate junction (Barberis & Molton 1995). These must suffice, within the space available, to indicate basic model performance and to give examples of the difficulties encountered in arriving at secure conclusions.

(*a*) *Diffuser*

The asymmetric diffuser involves separation from the inclined plane wall and reattachment in the constant-area duct following the expansion. This case has been specifically designed for validation and offers accurate and well-resolved mean-flow and turbulence data for well-controlled two-dimensional conditions. Importantly, it includes detailed data well removed from the diffuser section, allowing boundary conditions to be prescribed with a high level of confidence. The diffuser length is 21 times the upstream channel height H, and the overall expansion ratio is 4.7. The Reynolds number based on upstream-channel conditions is 21 200. Following grid-independence studies, the flow was computed with a second-order *total variation diminishing* (TVD) scheme and a 272×82 grid, extending $11H$ and $40H$ upstream and downstream of the diffuser section, respectively. The y^+ value along the gridline closest to the wall was below 1 throughout. Results presented here have been taken from studies by Apsley *et al.* (1997) and Apsley & Leschziner (1998).

Figure 6 shows the development of the streamwise mean velocity profile along the diffuser. Results have been included for one linear and two cubic low-*Re* eddy-viscosity models and the Reynolds-stress-transport model of Speziale *et al.* (1991), with the near-wall sublayer resolved by the one-equation model of Norris & Reynolds (1975). The linear EVM predicts a symmetric mean-velocity profile across the diffuser and near-isotropy amongst the normal-stress components (not shown). The addition of quadratic terms, as done by Speziale *et al.* (1991), distinguishes the individual normal stresses, but fails to improve the mean-velocity predictions significantly. In contrast, the cubic model of Apsley & Leschziner (1998), which combines (S, Ω)-dependent coefficients and nonlinear terms in the stress–strain relationship, provides a satisfactory prediction of cross-channel asymmetry, close to that achieved with the second-moment model. Good agreement is also returned in respect of normal and shear stresses, which are not included here.

(*b*) *Double-circular-arc (DCA) blade*

The DCA blade is formed by two circular arcs, joined by rounded, but thin, leading and trailing edges. The flow enters the blade passage at an angle that departs by

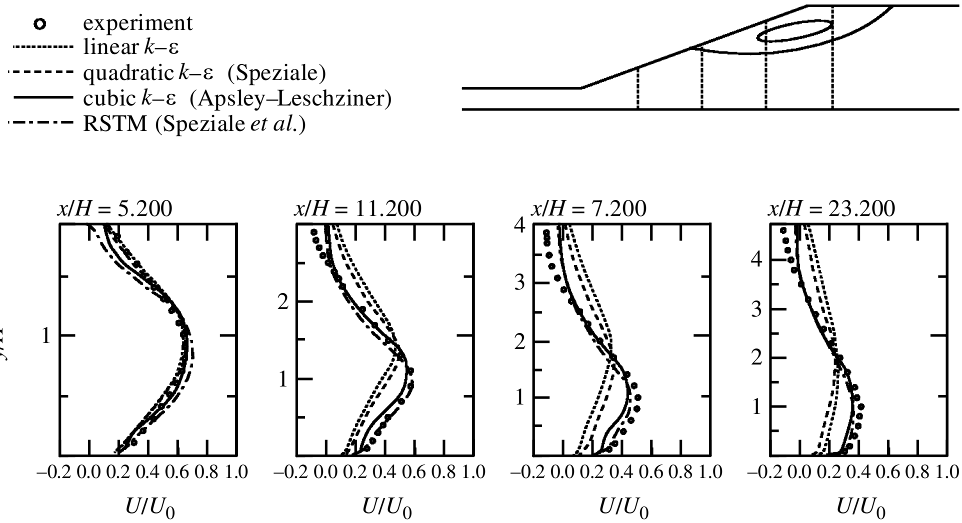

Figure 6. Streamwise velocity profiles in an asymmetric diffuser predicted with a linear EVM, two nonlinear EVMs and a second-moment model.

1.5° from the design value. This case, while disadvantageous in operational terms, is interesting in the context of turbulence modelling, as the flow on the blade's suction side is subjected to high levels of surface curvature and adverse pressure gradient. This results in a rapid growth of the suction-side boundary layer, leading to a large separation region towards the trailing edge and a strong interaction between the boundary layer and the passage flow. Unlike many other turbomachine-blade flows, the present case is not strongly influenced by transition. Thus, on the all-important suction side, transition occurs very close to the leading edge, possibly induced by a tiny leading-edge separation bubble. However, in the pressure-side boundary layer, which is subjected to acceleration and is thus thin and far less interesting than its suction-side counterpart, transition occurs at around 40% of chord.

The computational solutions presented here were obtained by Chen & Leschziner (1999) on a multi-block grid containing close to 50 000 nodes, with the linear EVM of Launder & Sharma (1974), the NLEVM of Craft *et al.* (1997*b*) and the second-moment closure of Gibson & Launder (1978), the last used in conjunction with the NLEVM to bridge the semi-viscous sublayer close to the wall. Figure 7 presents surface-pressure distributions, suction-side velocity profiles and distributions of boundary-layer displacement thickness. The existence of separation is implied by the pressure plateau located between *ca.* 80% of the chord and the trailing edge. Only the second-moment closure returns a credible prediction of the separation process, and this reflects its greater sensitivity to streamline curvature and the lower level of mixing it predicts in the boundary layer in the presence of adverse pressure gradient. The velocity profiles close to the leading edge indicate that neither the second-moment closure nor the linear EVM captures the transitional state of the leading-edge flow. However, as stated earlier, this is not a crucially important issue in this flow. As the flow progresses beyond the immediate leading-edge region, the linear model predicts an excessively turbulent boundary layer which is not sufficiently sensitive to adverse pressure gradient and which therefore remains attached. In con-

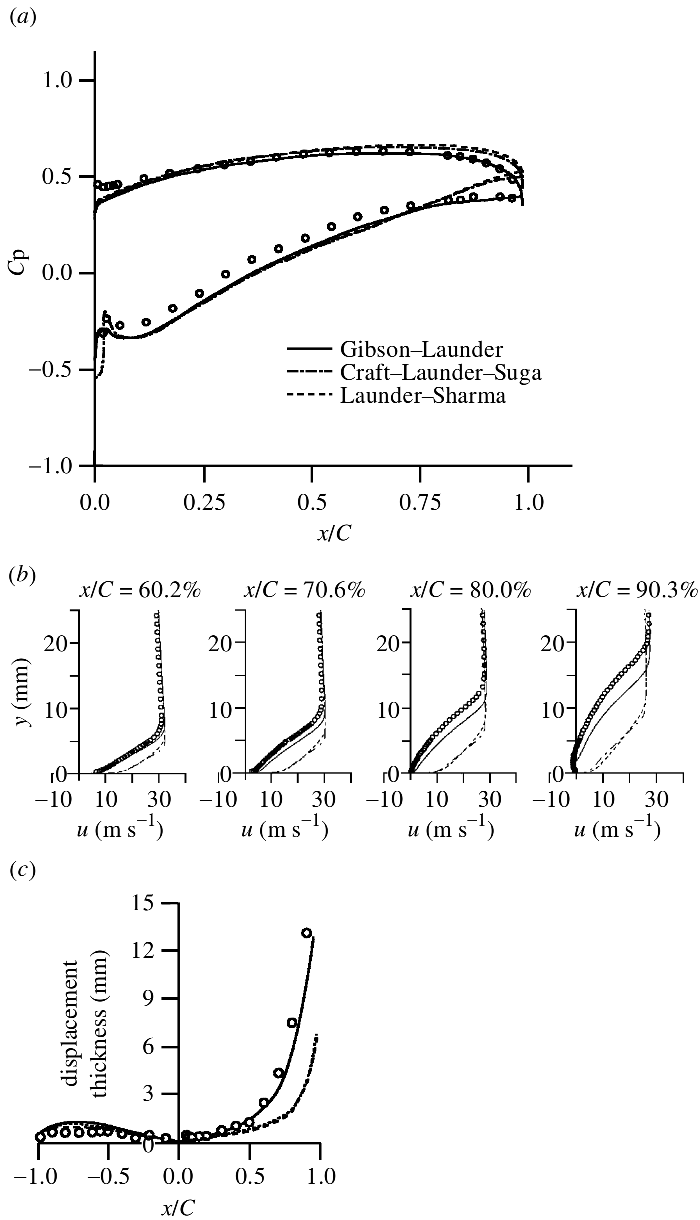

Figure 7. Flow over a DCA compressor-cascade blade predicted with a linear EVM, a cubic EVM and a second-moment model; (*a*) surface pressure, (*b*) suction-side streamwise velocity; (*c*) boundary-layer displacement thickness.

trast, the boundary layer returned by the second-moment closure grows rapidly, in accordance with experiment, and eventually separates at *ca.* 80% of the chord. As regards the NLEVM, despite the use of the elaborate stress–strain relation, the model fails to capture the trailing-edge separation, returning results which are no better than the linear model in the trailing-edge region. However, the root of its failure is different from that of the linear EVM, being a consequence of an overestimation of the leading-edge separation bubble. In the experiment, the boundary layer reattaches in a fully turbulent state at 3% of the chord. In contrast, the predicted boundary layer reattaches just upstream of the first measurement section at 7.3%. This results in a serious underestimation of the initial displacement thickness and turbulence intensity. With the wrong initial profiles, there arises a wrong response of the boundary layer to the pressure field further downstream. Although the nonlinear model is sensitive to streamline curvature, by virtue of its cubic fragments, this sensitivity is perhaps insufficiently strong, and may be a contributory factor in the model's failure. The superior performance of the second-moment closure, relative to the other two models, is brought out especially well by the distributions of the displacement thickness.

(*c*) *Prolate spheroid*

This is a flow around an elliptical body of revolution of axes ratio of 6:1 and inclined at 10° and 30° to an oncoming uniform stream. The geometry represents the group of external flows around streamlined bodies, which feature vortical separation that arises from an oblique 'collision' and subsequent separation of boundary layers from the body's leeward side. Of the two flows, that at 30° and $Re = 6.5 \times 10^6$ (based on chord) is much more challenging, but poses significant uncertainties due to a complex pattern of natural transition on the windward surface. Computations for both 10° and 30° incidence were performed by Lien & Leschziner (1996, 1997) with the low-*Re* linear EVM of Lien & Leschziner (1994), a low-*Re* adaptation of Shih *et al*.'s (1993) quadratic EVM, and the second-moment closure of Gibson & Launder (1978), the last coupled to the above linear EVM in the viscous sublayer. A second-order TVD scheme was used on a high-quality conformal mesh of $98 \times 82 \times 66$ nodes, with the y^+ value closest to the wall being kept to 0.5–1 across the entire surface. Although this mesh resolves most properties adequately, test calculations with a nonlinear EVM on a 128^3 grid have shown the skin friction to change slightly with grid refinement.

Figure 8 contains comparisons for skin-friction lines on the unwrapped spheroid surface, one azimuthal pressure distribution, one distribution of skin-friction direction and one velocity field, the last showing the leeward separation and the associated transverse vortex. In general, the NLEVM and the second-moment closure give similar results that are closer to the experiments than those obtained with the linear EVM. However, the improvement is not dramatic, and the uncertainties associated with transition do not warrant a definitive statement on model performance in this very complex case.

(*d*) *Circular bump*

This geometry consists of a solid cylinder with a circular arc bump, subjected to an $M = 0.875$ approach flow. The bump accelerates the flow, locally, to $M = 1.4$, and the flow then returns to a subsonic state through a strong shock which causes the boundary layer to separate. This is, therefore, a searching test for the ability of turbulence models to represent shock–boundary-layer interaction.

A 180×110 grid was used, with clustering applied around the shock and near the wall, the y^+ value along the gridline closest to the wall being of the order of 0.5 throughout. Computational results obtained by Loyau *et al*. (1998) and Batten *et al*.

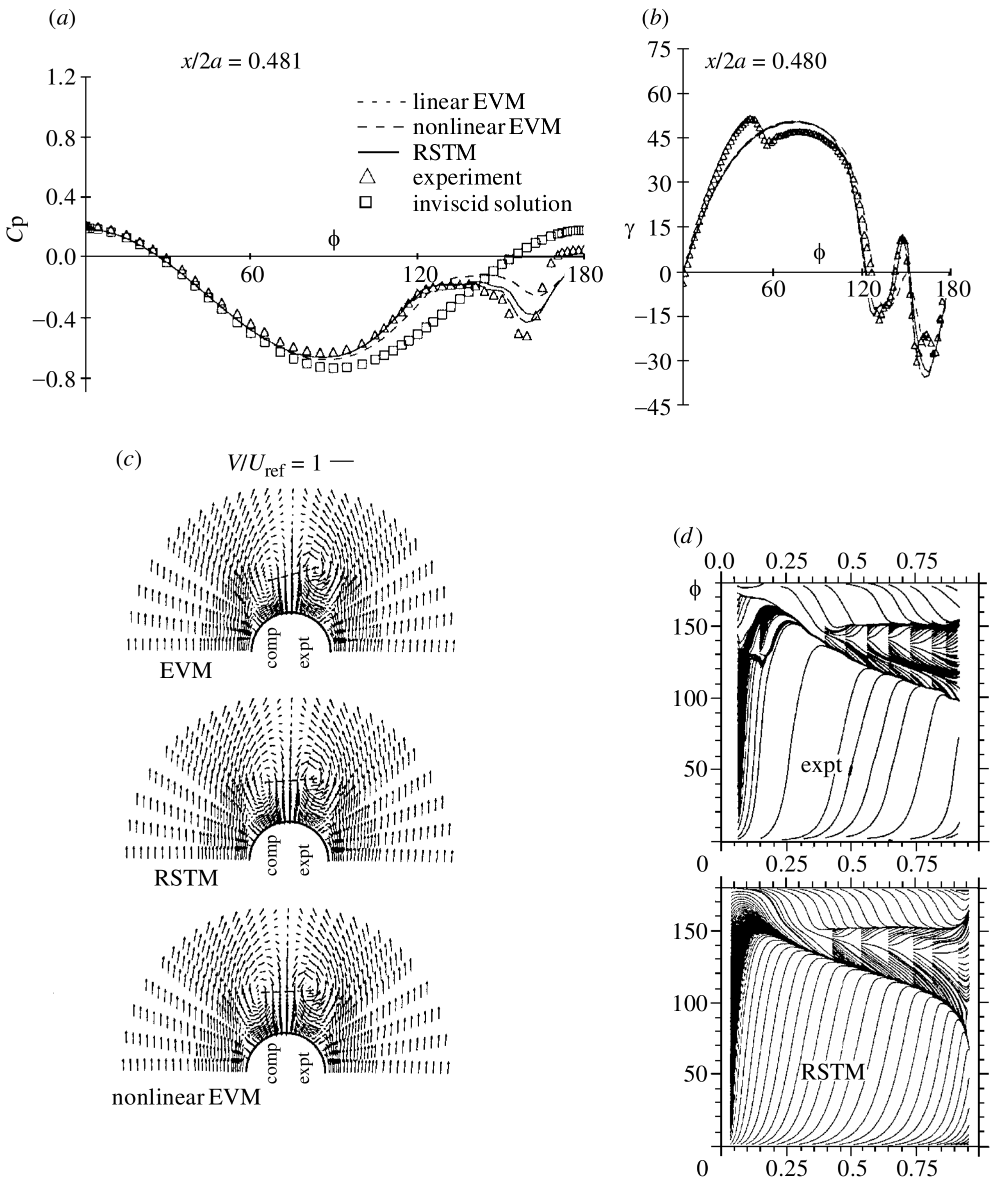

Figure 8. Flow around a prolate spheroid at 30° incidence predicted with a linear EVM and non-linear EVM and a second-moment model; (*a*) azimuthal variation of wall pressure; (*b*) azimuthal variation of skin-friction direction; (*c*) transverse velocity above leeward portion of the spheroid; (*d*) skin-friction lines.

(1999) for different models are compared in figure 9 with experimental data. Several NLEVMs and second-moment closure models feature in the comparisons, and are designated as follows: WR, Wilcox & Rubesin (1980); CLS, Craft *et al.* (1997*b*); AL, Apsley & Leschziner (1998); JH, Jakirlić & Hanjalić (1995); MCL, Craft & Launder (1996), Batten *et al.* (1999); SST, Menter (1994), a linear model with a vorticity-

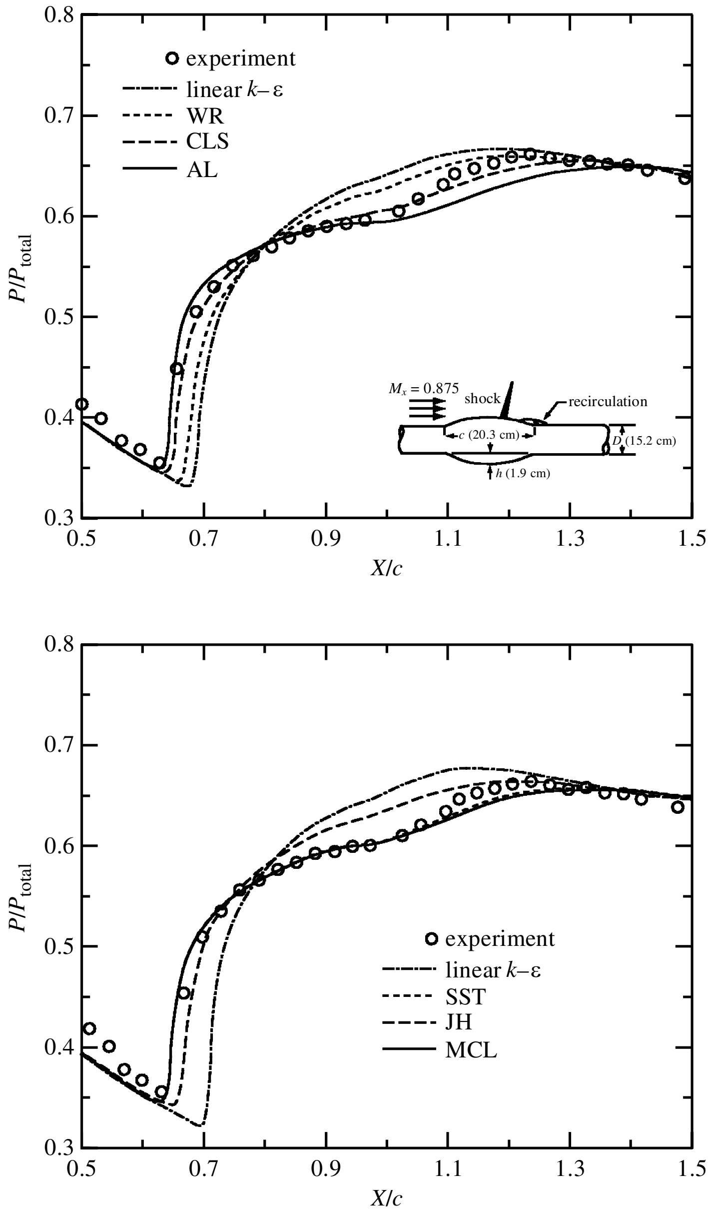

Figure 9. Wall-pressure variations along cylindrical bump subjected to transonic flow with shock-induced boundary-layer separation; predictions with two linear EVMs, three nonlinear EVMs and two second-moment models.

sensitized form of c_μ (see figure 5). The cubic AL model and the MCL second-moment closure are seen to return a considerably more pronounced pressure-plateau region than do other models, predicting a shock location which is fractionally too far upstream. The SST (*shear stress transport*) model—essentially a linear EVM—gives a performance very similar to the best nonlinear eddy-viscosity and second-moment models, but this is due, in large measure, to the use of a vorticity-sensitized form of

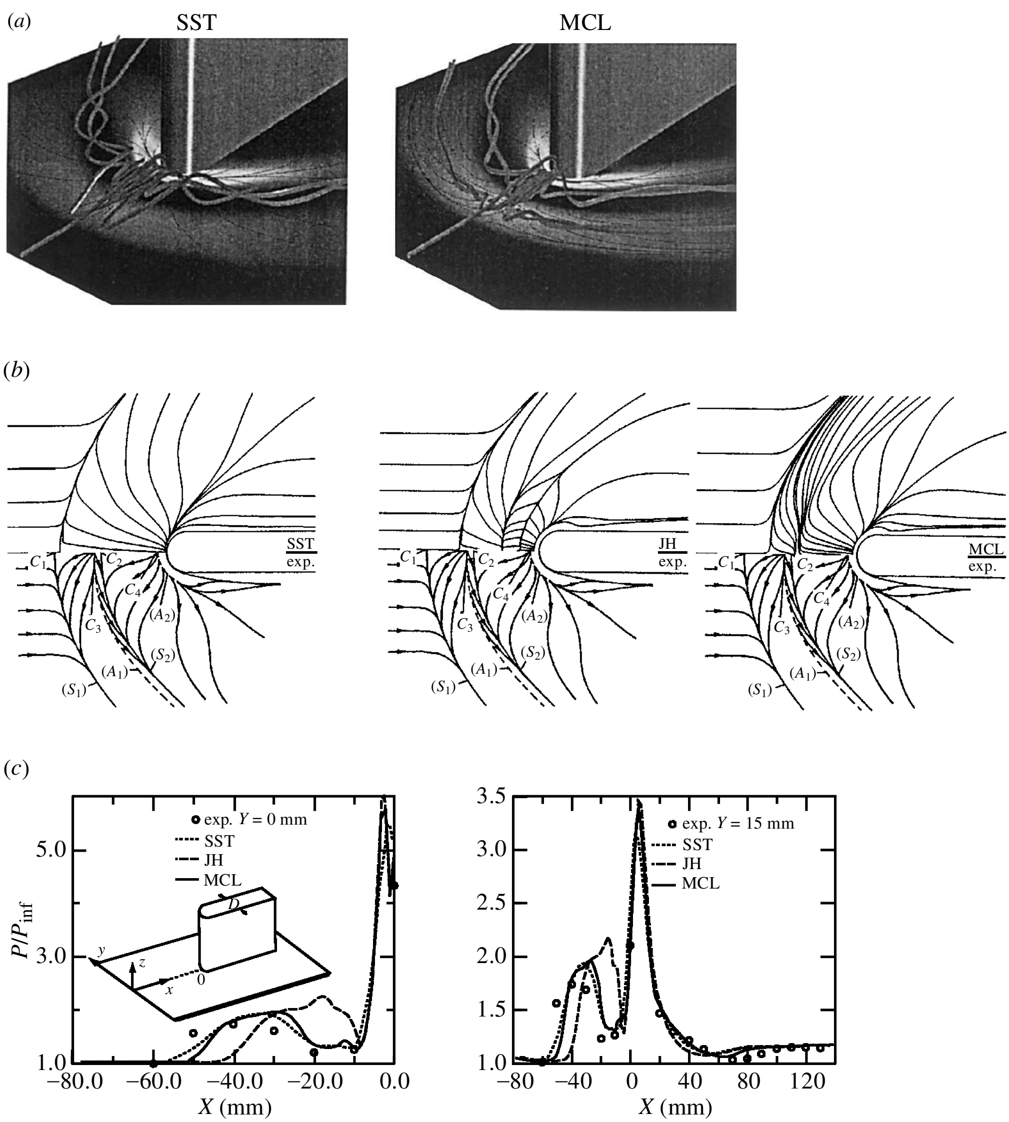

Figure 10. Mach 2 flow around a wall-mounted fin predicted with Menter's (1994) SST model and two Reynolds-stress models; (*a*) structure of post-shock horseshoe vortex; (*b*) vortex footprint on flat wall in terms of skin-friction lines; (*c*) streamwise wall-pressure variations at two transverse locations.

c_μ and a carefully crafted shear-stress limiter. Comparisons for velocity and shear-stress profiles may be found in Batten *et al.* (1999) and Loyau *et al.* (1998) and are, in terms of sensitivity to the shock, consistent with the results for the pressure.

(*e*) *Fin–plate junction*

In this flow, shown in figure 10, a Mach 2 flat-plate boundary layer collides with the rounded normal fin, producing a complex shock–boundary-layer interaction and multiple horse-shoe vortices. Experimental data for surface pressure, velocity, (LDA) skin-friction patterns and Reynolds stresses have been obtained by Barberis & Molton (1995). While the geometry and flow are well controlled, uncertainties arise because of a lack of detail in the measured boundary layer well upstream of the fin (only its thickness was given) and the presence of leakage between the fin tip and the upper wall of the wind tunnel. The latter poses some uncertainty about the boundary conditions on the upper computational boundary, which is a virtual plane parallel to, and well-removed from, the lower wall.

Computations have been performed by Batten *et al.* (1999) on an $80 \times 80 \times 70$ C-type grid surrounding the fin, with the y^+ value closest to the wall being of the order of 0.5. Several low-*Re* linear EVMs, Menter's (1994) linear SST EVM and three low-*Re* second-moment closures (Launder & Shima 1989; Jakirlić & Hanjalić 1995; Batten *et al.* 1999), have been examined. A few results arising from the models of Menter (1994), Jakirlić & Hanjalić (1995) and Batten *et al.* (1999) (denoted, as in the previous case, by SST, JH and MCL, respectively) are given in figure 10, and these illustrate that only the second-moment closure is able to reproduce the multiple separation/reattachment structure ahead of the fin that is observed in the experiment, although the patterns are not identical. All models tend to underestimate, some by a substantial margin, the size of the separated region upstream of the fin. Indeed, different variants of second-moment closure return significantly different results, and this illustrates the often-observed high sensitivity of the performance of second-moment models to the details of approximating the pressure–strain-interaction and dissipation processes. In common with the previous case, the linear SST EVM results, here too, in pressure distributions that are as good as those returned by the second-moment models. However, it must be noted again that the SST model is carefully tuned and contains a highly influential limiter, which depresses the shear stress in certain regions of the flow, thus enhancing separation and enlarging the size of separated zones. In contrast, second-moment closure aims to achieve agreement with reality by increasing the level of generality and fundamental rigour of the equations describing the physics of turbulence.

6. Concluding remarks

Much effort has been put, over the past few years, into the construction, calibration and validation of improved forms of second-moment closure and nonlinear eddy-viscosity models. This is an especially difficult area of CFD, and progress is much slower than that on the numerical front. Difficulties with stable and accurate model implementation, the fine grids and high CPU resources required, the lack of sufficiently accurate and well-resolved data derived from well-controlled experiments, and the small number of groups engaged and collaborating in advanced modelling (especially that involving three-dimensional flows) make validation very challenging and its outcome subject to much uncertainty.

There is no doubt that, from a fundamental point of view, second-moment closure is superior to NLEVMs. This superiority is rooted, in large measure, in the exact representation of stress generation, which involves an intricate interplay between all stress and strain components. On the other hand, the need to model the influential process of turbulence-energy redistribution and reduction of the shear component in harmony with isotropization is, in practice, a potent source of variability in performance. Added to this, second-moment closure poses not inconsiderable numerical challenges and entails relatively high computational costs.

NLEVMs have sprung from the desire to circumvent the complexities and numerical difficulties associated with second-moment closure. While the nonlinear fragments sensitize the models to normal-stress anisotropy and curvature strain, the mechanisms by which this sensitivity is established are materially different from the actual physical interactions which are represented by the exact stress-generation terms in the Reynolds-stress-transport equations. These fundamental differences are accentuated by the fact that nonlinear models imply no causal relationship between anisotropy and sensitivity to curvature. Moreover, the weak response of turbulence energy to irrotational straining—in reality, again rooted in stress-production terms—can only be captured by nonlinear models through a functional dependence of the eddy-viscosity coefficient, c_μ, on strain and vorticity invariants. The fact that materially different nonlinear forms arise from alternative approaches to their derivation, and the extensive dependence of these models on calibration, are reasons for the substantial variability in performance observed when the models are applied even to relatively simple flows.

Notwithstanding the rather subdued view conveyed by the above remarks, the considerable number of computational studies reported in the open literature justifies the overall observation that anisotropy-resolving closures offer not insubstantial predictive advantages over simpler closures in complex strain fields. In general, the advantages in three-dimensional flow appear to be less pronounced than in two-dimensional ones (at least in terms of the dynamic state). While this observation might initially appear curious, a possible explanation may lie in the fact that turbulent transport in three-dimensional flows tends to be less dominant, relative to inviscid contributions, than in two-dimensional ones. This is linked to higher levels of flow curvature present in many complex three-dimensional flows, with which convective transport and pressure gradients are associated.

References

Apsley, D. D. & Leschziner, M. A. 1998 A new low-*Re* non-linear two-equation turbulence model for complex flows. *Int. J. Heat Fluid Flow* **19**, 209–222.

Apsley, D. D., Chen, W.-L., Leschziner, M. A. & Lien, F.-S. 1997 Non-linear eddy-viscosity modelling of separated flows. *IAHR J. Hydraulic Res.* **35**, 723–748.

Bachalo, W. D. & Johnson, D. A. 1986 Transonic turbulent boundary layer separation generated on an axisymmetric flow model. *J. AIAA* **24**, 437–443.

Barberis, D. & Molton, P. 1995 Shock wave–turbulent boundary layer interaction in a three dimensional flow. In *Proc. 33rd Aerospace Sciences Mtg and Exibit, Reno, NV, USA*, paper AIAA-95-0227.

Batten, P., Craft, T. J., Leschziner, M. A. & Loyau, H. 1999 Reynolds-stress-transport modelling for compressible aerodynamic flows. *J. AIAA* **37**, 785–796.

Chen, W.-L. & Leschziner, M. A. 1999 Modelling turbomachine-blade flows with non-linear eddy-viscosity models and second-moment closure. In *Proc. 3rd Eur. Conf. on Turbomachinery: Fluid Dynamics and Thermodynamics, IMechE Conf. Trans.*, paper C557/131/99, pp. 189–199.

Craft, T. J. 1998 Developments in a low-Reynolds-number second-moment closure and its application to separating and reattaching flows. *Int. J. Heat Fluid Flow* **19**, 541–548.

Craft, T. J. & Launder, B. E. 1992 New wall-reflection model applied to the turbulent impinging jet. *J. AIAA* **30**, 2970–2972.

Craft, T. J. & Launder, B. E. 1996 A Reynolds stress closure designed for complex geometries. *Int. J. Heat Fluid Flow* **17**, 245–254.

Craft, T. J., Kidger, J. W. & Launder, B. E. 1997*a* Importance of third-moment modelling in horizontal, stably-stratified flows. In *Proc. 11th Shear Flows Symp., Grenoble*, pp. 20.13–20.18.

Craft, T. J., Launder, B. E. & Suga, K. 1997*b* Prediction of turbulent transitional phenomena with a nonlinear eddy-viscosity model. *Int. J. Heat Fluid Flow* **18**, 15–28.

Daly, B. J. & Harlow, F. H. 1970 Transport equations in turbulence. *Phys. Fluids* **13**, 2634–2649.

Demuren, A. O. & Sarkar, S. 1993 Perspective: systematic study of Reynolds-stress closure models in the computation of plane channel flows. *ASME J. Fluids Engng* **115**, 5–12.

Durbin, P. A. 1993 A Reynolds stress model for near-wall turbulence. *J. Fluid Mech.* **249**, 465–498.

Eggels, J. G. M., Unger, F., Weiss, M. H., Westerweel, J., Adrian, R. J., Friedrich, R. & Nieuwstadt, F. T. M. 1994 Fully developed turbulent pipe flow: a comparison between direct numerical simulation and experiment. *J. Fluid Mech.* **268**, 175–209.

Ellis, L. B. & Joubert, P. N. 1974 Turbulent shear flow in a curved duct. *J. Fluid Mech.* **62**, 65–84.

Fu, S., Launder, B. E. & Tselepidakis, D. P. 1987*a* Accommodating the effects of high strain rates in modelling the pressure–strain correlation. Report TFD/87/5, University of Manchester Institute of Science and Technology, Mechanical Engineering Department.

Fu, S., Leschziner, M. A. & Launder, B. E. 1987*b* Modelling strongly swirling recirculating jet flow with Reynolds-stress transport closure. In *Proc. 6th Symp. on Turbulent Shear Flow, Toulouse*, pp. 17.6.1–17.6.6.

Gatski, T. B. & Speziale, C. G. 1993 On explicit algebraic stress models for complex turbulent flows. *J. Fluid Mech.* **254**, 59–78.

Gibson, M. M. & Launder, B. E. 1978 Ground effects on pressure fluctuations in the atmospheric boundary layer. *J. Fluid Mech.* **86**, 491–511.

Haase, W., Brandsma, F., Elsholz, E., Leschziner, M. A. & Schwamborn, D. (eds) 1993 EUROVAL—a European initiative on validation of CFD codes—results of the EC/BRITE-EURAM project EUROVAL 1990–1992. *Notes on Numerical Fluid Mechanics* vol. 42. Braunschweig: Vieweg.

Haase, W., Chaput, E., Elsholz, E., Leschziner, M. A. & Müller, U. R. 1996 ECARP: European computational aerodynamics research project. II. Validation of CFD codes and assessment of turbulent models. *Notes on Numerical Fluid Mechanics* vol. 58. Braunschweig: Vieweg.

Hanjalić, K. 1994 Advanced turbulence closure models: a view of current status and future prospects. *Int. J. Heat Fluid Flow* **15**, 178–203.

Hanjalić, K. & Jakirlić, S. 1993 A model of stress dissipation in second moment closures. *Appl. Sci. Res.* **51**, 513–518.

Haroutunian, V., Ince, N. & Launder, B. E. 1988 A new proposal for the ε equation. In *Proc. 3rd UMIST CFD Colloquium, UMIST, Manchester*, p. 1.3.

Ince, N. Z., Betts, P. L. & Launder, B. E. 1994 Turbulent natural convection in enclosures. In *Proc. EUROTHERM Seminar 22* (ed. R. A. W. M. Henkes & C. J. Hoogendoorn), p. 76.

Jakirlić, S. 1997 Reynolds-spannungs-modellierung komplexer turbulenter Stroemungen. PhD thesis, University of Erlangen, Nürnberg.

Jakirlić, S. & Hanjalić, K. 1995 A second-moment closure for non-equilibrium and separating high- and low-*Re*-number flows. In *Proc. 10th Symp. on Turbulent Shear Flows, Pennsylvania State University*, pp. 23.25–23.30.

Kim, J., Moin, P. & Moser, R. 1987 Turbulence statistics in fully-developed channel flow at low Reynolds number. *J. Fluid Mech.* **177**, 133–166.

Launder, B. E. & Reynolds, W. C. 1983 Asymptotic near-wall stress dissipation rates in a turbulent flow. *Phys. Fluids* **26**, 1157–1158.

Launder, B. E. & Sharma, B. I. 1974 Application of the energy-dissipation model of turbulence to the calculation of flow near a spinning disc. *Lett. Heat Mass Transfer* **1**, 131–138.

Launder, B. E. & Shima, N. 1989 Second-moment closure for the near-wall sublayer. *J. AIAA* **27**, 1319–1325.

Launder, B. E. & Tselepidakis, D. P. 1993 Contribution to the modelling of near-wall turbulence. In *Turbulent shear flows* (ed. F. Durst *et al.*), vol. 8, pp. 81–96. Springer.

Launder, B. E., Reece, G. J. & Rodi, W. 1975 Progress in the development of Reynolds-stress turbulence closure. *J. Fluid Mech.* **68**, 537–566.

Le, H. & Moin, P. 1994 Direct numerical simulation of turbulent flow over a backward-facing step. Report no. TF-58, Department of Mechanical Engineering, Stanford University, CA, USA.

Lee, M. J. & Reynolds, W. C. 1985 Numerical experiments on the structure of homogeneous turbulence. Report no. TF-24, Department of Mechanical Engineering, Stanford University, CA, USA.

Leschziner, M. A. & Ince, N. Z. 1995 Computational modelling of three-dimensional impinging jets with and without cross flow using second-moment closure. *Comp. Fluids* **24**, 811–832.

Lien, F. S. 1992 Computational modelling of 3D flow in complex ducts and passages. PhD thesis, University of Manchester, UK.

Lien, F. S. & Durbin, P. A. 1996 Non-linear k–v^2 modelling with application to high-lift. In *Proc. Summer Program, Centre For Turbulence Research, Stanford University*, pp. 5–22.

Lien, F.-S. & Leschziner, M. A. 1993 Modelling 2D and 3D separation from curved surfaces with variants of second-moment closure combined with low-*Re* near-wall formulations. In *Proc. 9th Symp. Turbulent Shear Flows, Kyoto*, pp. 13.1.1–13.1.6.

Lien, F. S. & Leschziner, M. A. 1994 Modelling the flow in a transition duct with a non-orthogonal FV procedure and low-*Re* turbulence-transport models. In *ASME Summer Mtg, FED Symp. on Advances in Computational Methods in Fluid Dynamics*, pp. 93–106.

Lien, F. S. & Leschziner, M. A. 1995 Modelling 2D separation from high-lift aerofoils with a non-linear eddy-viscosity model and second-moment closure. *Aeronaut. J.* **99**, 125–144.

Lien, F. S. & Leschziner, M. A. 1996 Second-moment closure for three-dimensional turbulent flow around and within complex geometries. *Comp. Fluids* **25**, 237–262.

Lien, F. S. & Leschziner, M. A. 1997 Computational modelling of separated flow around streamlined body at high incidence. *Aeronaut. J.* **101**, 269–275.

Lien, F. S., Chen, W. L. & Leschziner, M. A. 1996 Low-Reynolds-number eddy-viscosity modelling based on non-linear stress-strain/vorticity relations. In *Engineering turbulence modelling and measurements* (ed. W. Rodi & G. Bergeles), vol. 3, pp. 91–100. Elsevier.

Loyau, H., Batten, P. & Leschziner, M. A. 1998 Modelling shock/boundary-layer interaction with non-linear eddy-viscosity closures. *J. Flow Turbulence Combust.* **60**, 257–282.

Lumley, J. L. 1978 Computational modelling of turbulent flows. *Adv. Appl. Mech.* **18**, 123–176.

Matsumoto, A., Nagano, Y. & Tsuji, T. 1991 Direct numerical simulation of homogeneous turbulent shear flows. In *Proc. 5th Symp. on Computational Fluid Dynamics*, pp. 361–364.

Meier, H. U., Kreplin, H. P., Landhauser, A. & Baumgarten, D. 1984 Mean velocity distribution in 3D boundary layers developing on a 1:6 prolate spheroid with artificial transition. Deutsche Forschungsverein für Luft und Raumfahrt report IB 222–84 A11.

Menter, F. R. 1994 Two equation eddy viscosity turbulence models for engineering applications. *J. AIAA* **32**, 1598–1605.

Moin, P. & Kim, J. 1997 Tackling turbulence with supercomputers. *Scientific American* **276**, 62–68.

Norris, L. H. & Reynolds, W. C. 1975 Turbulence channel flow with a moving wavy boundary. Report FM-10, Department of Mechanical Engineering, Stanford University, CA, USA.

Obi, S., Aoki, K. & Masuda, S. 1993 Experimental and computational study of turbulent separated flow in an asymmetric diffuser. In *Proc. 9th Symp. on Turbulent Shear Flows, Kyoto*, vol. 3, p. 305.

Pope, S. B. 1975 A more general effective-viscosity hypothesis. *J. Fluid Mech.* **72**, 331–340.

Rivlin, R. S. 1957 The relation between the flow of non-Newtonian fluids and turbulent Newtonian fluid. *Q. Appl. Math.* **15**, 212–215.

Rodi, W. 1976 A new algebraic relation for calculating the Reynolds stresses. *Z. Angew. Math. Mech.* **56**, 219–221.

Rotta, J. C. 1951 Statistische Theory nichhomogener Turbulenz. *Z. Phys.* **129**, 547–572.

Rubinstein, R. & Barton, J. M. 1990 Non-linear Reynolds stress models and the renormalisation group. *Phys. Fluids* A **2**, 1472–1476.

Saffman, P. G. 1977 Results of a two-equation model for turbulent flows and development of a relaxation stress model for application to straining and rotating flows. In *Proc. Project SQUID Workshop on Turbulence in Internal Flows* (ed. S. Murthy), pp. 191–231. New York: Hemisphere.

Shih, T. H. & Lumley, J. L. 1985 Modelling of pressure correlation terms in Reynolds-stress and scalar-flux equations. Report FDA-85–3, Sibley School of Mechanics and Aerospace Engineering, Cornell University, NY, USA.

Shih, T.-H., Zhu, J. & Lumley, J. L. 1993 A realisable Reynolds stress algebraic equation model. NASA report TM105993.

Shir, C. C. 1973 A preliminary numerical study of atmospheric turbulent flows in the idealized planetary boundary layer. *J. Atmos. Sci.* **30**, 1327–1333.

So, R. M. C., Lai, Y. G., Zhang, H. S. & Hwang, B. C. 1991 Second-order near-wall turbulence closures: a review. *J. AIAA* **29**, 1819–1835.

Spalart, P. R. 1988 Direct numerical simulation of a turbulent boundary layer up to $R = 1410$. *J. Fluid Mech.* **187**, 61–98.

Spalart, P. R. & Baldwin, B. S. 1989 Direct numerical simulation of a turbulent oscillating boundary layer. In *Turbulent shear flows* (ed. J. C. André *et al.*), vol. 6, pp. 417–440. Springer.

Speziale, C. G. 1987 On nonlinear K–l and K–ε models of turbulence. *J. Fluid Mech.* **178**, 459–475.

Speziale, C. G., Sarkar, S. & Gatski, T. B. 1991 Modelling the pressure-strain correlation of turbulence: an invariant dynamical systems approach. *J. Fluid Mech.* **227**, 245–272.

Taulbee, D. B., Sonnenmeier, J. R. & Wall, K. M. 1993 Application of a new non-linear stress–strain model to axisymmetric turbulent swirling flows. In *Engineering turbulence modelling and experiments* (ed. W. Rodi & F. Martelli), vol. 2, pp. 103–112. Elsevier.

Tavoularis, S. & Corrsin, S. 1981 Experiment in nearly homogeneous turbulent shear flow with a uniform mean temperature gradient. Part I. *J. Fluid Mech.* **104**, 311–347.

Wallin, S. & Johansson, A. V. 1997 A new explicit algebraic Reynolds stress turbulence model for 3D flows. In *Proc. 11th Symp. on Turbulent Shear Flows, Grenoble* (ed. F. Durst *et al.*), pp. 13.13–13.17.

Wilcox, D. C. 1994 Simulation transition with a two-equation turbulence model. *J. AIAA* **32**, 247–255.

Wilcox, D. C. & Rubesin, M. W. 1980 Progress in turbulence modelling for complex flow field including effects of compressibility. NASA report TP1517.

Yap, C. R. 1987 Turbulent heat and momentum transfer in recirculating and impinging flows. PhD thesis, University of Manchester, UK.

Yoshizawa, A. 1987 Statistical analysis of the derivation of the Reynolds stress from its eddy-viscosity representation. *Phys. Fluids* **27**, 1377–1387.

Zierke, W. C. & Deutsch, S. 1989 The measurement of boundary layers on a compressor blade in a cascade. NASA report CR-185118.